

1 **Evaluating MODIS snow products using an extensive wildlife camera network**

2

3 **Catherine Breen¹, Carrie Vuyovich², John Odden³, Dorothy Hall⁴, Laura Prugh¹**

4 ¹ Department of Environmental and Forest Sciences, University of Washington, Seattle WA
5 USA

6 ² Hydrological Sciences Laboratory, NASA Goddard Space Flight Center, Greenbelt, MD,
7 USA.

8 ³ Norwegian Institute for Nature Research, Post Office Box 5685 Sluppen, 7485 Trondheim,
9 Norway.

10 ⁴ Earth System Science Interdisciplinary Center, University of Maryland College Park,
11 College Park, MD, USA.

12

13 Corresponding author: Catherine Breen, Department of Environmental and Forest Sciences,

14 University of Washington, Seattle WA 98195. Email: cbreen@uw.edu, <https://orcid.org/0000->

15 [0001-9597-2061](https://orcid.org/0001-9597-2061)

16

17

18 **Abstract**

19 Snow covers a maximum of 47 million km² of Earth's northern hemisphere each winter
20 and is an important component of the planet's energy balance, hydrology cycles, and ecosystems.
21 Monitoring regional and global snow cover has increased in urgency in recent years due to
22 warming temperatures and declines in snow cover extent. Optical satellite instruments provide
23 large-scale observations of snow cover, but cloud cover and dense forest canopy can reduce
24 accuracy in mapping snow cover. Remote camera networks deployed for wildlife monitoring
25 operate below cloud cover and in forests, representing a virtually untapped source of snow cover
26 observations to supplement satellite observations. Using images from 1,181 wildlife cameras
27 deployed by the Norwegian Institute for Nature Research (NINA), we compared snow cover
28 extracted from camera images to Moderate Resolution Imaging Spectroradiometer (MODIS)
29 snow cover products during winter months of 2018-2020. Ordinal snow classifications (scale =
30 0-4) from cameras were closely related to normalized difference snow index (NDSI) values from
31 the MODIS Terra Snow Cover Daily L3 Global 500m (MOD10A1) Collection 6 product ($R^2 =$
32 0.70). Tree canopy cover, the normalized difference vegetation index (NDVI), and image color
33 mode influenced agreement between camera images and MOD10A1 NDSI values. For
34 MOD10A1F, MOD10A1's corresponding cloud-gap filled product, agreement with cloud-gap
35 filled values decreased from 78.5% to 56.4% in the first three days of cloudy periods and
36 stabilized thereafter. Using our camera data as validation, we derived a threshold to create daily
37 binary maps of snow cover from the MOD10A1 product. The threshold corresponding to snow
38 presence was an NDSI value of 40.50, which closely matched a previously defined global binary
39 threshold of 40 using the MOD10A2 8-day product. These analyses demonstrate the utility of

Breen, Catherine; Vuyovich, Carrie; Odden, John; Hall, Dorothy; Prugh, Laura.
Evaluating MODIS snow products using an extensive wildlife camera network. *Remote Sensing of Environment* 2023 ;Volum 295. s. - [10.1016/j.rse.2023.113648](https://doi.org/10.1016/j.rse.2023.113648)

40 camera trap networks for validation of snow cover products from satellite remote sensing, as
41 well as their potential to identify sources of inaccuracy.

42 Keywords: validation, Norway, remote cameras, gap-filling, MODIS, snow

43

44 **Introduction**

45 Seasonal snow covers 31% of the Earth's land surface each year, playing an integral role
46 in habitat quality for wildlife, water storage for hydrological processes, and human uses such as
47 agriculture, forestry, and tourism (Mankin et al., 2015; Rizzi et al., 2018). Warming temperatures
48 have reduced snow cover extent globally, but these changes vary strongly among regions (Brown
49 and Mote, 2009; Solomon et al., 2007). Accurate snow cover mapping within and across years is
50 thus needed to inform regional forecasting and climate change mitigation efforts.

51 Snow cover is typically measured using ground observations, modeling, and remote
52 sensing at scales that range from point measurements (e.g., ground observations) to kilometers
53 (e.g., passive microwave sensors at 25-km resolution). Remote sensing from satellites is a
54 powerful tool because satellites provide information across broad spatial coverages and at fine
55 temporal scales, enabling global and regional snow cover maps where *in situ* measurements may
56 not be possible (Nolin, 2010). NASA's Moderate Resolution Imaging Spectroradiometer
57 (MODIS) Collection 6 product provides a daily or every other day 500-m resolution optical
58 image from which snow maps are derived. Daily MODIS snow observations are highly suitable
59 for continuous snow monitoring, which is desirable for many applications, including wildlife
60 science (Boelman et al., 2019). For example, daily MODIS snow maps have been used to

61 successfully detect changes in bird nesting success and shifts in the timing of mammal
62 migrations (Laforge et al., 2021; Madsen et al., 2007).

63 The most recent version of the MODIS products (Collection 6.1) includes a daily 500-m
64 global snow product, MOD10A1, and a daily cloud-gap filled (CGF) 500-m global snow
65 product, MOD10A1F. Both are suitable for use as inputs in hydrological, ecological, and climate
66 models (Bokhorst, 2016; Dong and Menzel, 2016). MOD10A1 and MOD10A1F provide
67 normalized difference snow index (NDSI) values based on the high reflectance of snow in the
68 visible band and low reflectance in the near-infrared band, ranging from 0 (snow-free) to 100
69 (completely snow-covered). NDSI values lower than 100 can be completely snow-covered
70 (Klein et al., 1998), but adjusting NDSI values to a fractional snow cover is no longer included in
71 MODIS products as it is region-dependent and other factors may affect when MODIS
72 underestimates snow. The overall accuracy of the MOD10A1 product is estimated to fall
73 between 79.5- 96% depending on the tree cover density, snow depth, and solar zenith angle in
74 the region of interest (Coll and Li, 2018; Franklin, 2020; Hall et al., 2019a; Hall and Riggs,
75 2007). Optical sensors are obstructed by tree cover, and shallow snow might not be bright
76 enough to reflect solar radiation since the underlying material is likely to be darker (Liang et al.,
77 2008). At high solar zenith angles, chances are higher that sensors will be obstructed by clouds
78 and experience higher atmospheric distortion (Xin et al., 2012), both of which can also obscure
79 or scatter light, decreasing the accuracy of observations.

80 Cloud masking in MOD10A1 greatly reduces coverage (Hall et al., 2019a), and
81 MOD10A1F improves coverage by filling all cloud-masked pixels. Each cloud-masked pixel is
82 given the most recently observed snow cover value, along with a corresponding “cloud

83 persistence” value for the age in days of the snow observation. This product has been used in
84 applications such as hydrological snow trend studies (Hao et al., 2022) and analyses of snow
85 cover impacts on wildlife (Mahoney et al., 2018). The cloud-gap filled product has been shown
86 to return similar accuracy as MOD10A1 in the western US where cloudy periods are typically
87 brief (Hall et al., 2019a), whereas accuracy is lower in the northeastern and northwestern US
88 where longer cloudy periods are common (Gao et al., 2011; Hall et al., 2010). Beyond the US,
89 validation of the MOD10A1F product is sparse due to the recency of the product availability.
90 Weather stations and other sensors improved MOD10A1F maps in China (Hao et al., 2022), but
91 more work in diverse areas with longer cloudy episodes, such as high latitude regions, is needed
92 to understand the accuracy of the MOD10A1F product in those areas. Understanding accuracy
93 may inform a region-dependent threshold after which additional cloudy days may result in
94 unreliable snow cover estimates, and indicate when alternative sources for snow cover, such as
95 weather stations or other ground observations, should be used instead of gap-filled values.

96 Binary products can be developed from the current MODIS snow-cover products and
97 may be used to map snow presence/absence. Early MODIS snow-cover products categorized
98 pixels as “snow” if the NDSI was greater than 40, using Landsat fractional snow-covered area
99 maps from Prince Albert National Park in Saskatchewan, Canada (Klein et al., 1998). Later, a
100 binary map developed from MOD10A2 categorized a pixel as “snow” if any pixel within an 8-
101 day period had an NDSI value greater than 10 (Hall et al., 2002). The lower threshold increased
102 snow detection but at the cost of increased false positives. Now, the threshold for snow presence
103 is considered region dependent (Thapa et al., 2019; Zhang et al., 2019), and the end-user is
104 recommended to determine the threshold above which the corresponding pixel should be

Breen, Catherine; Vuyovich, Carrie; Odden, John; Hall, Dorothy; Prugh, Laura.
Evaluating MODIS snow products using an extensive wildlife camera network. *Remote Sensing
of Environment* 2023 ;Volum 295. s. - [10.1016/j.rse.2023.113648](https://doi.org/10.1016/j.rse.2023.113648)

105 identified as snow covered (Riggs et al., 2017). Given the utility of binary snow products for
106 monitoring snow phenology and subsequent applicability to wildlife studies (Curk et al., 2020;
107 Madsen et al., 2007; Thapa et al., 2019), more work is needed to develop daily binary snow maps
108 for specific regions.

109 In this study, we use cameras deployed in remote locations for wildlife monitoring, often
110 referred to as “camera traps,” to evaluate the MODIS/Terra MOD10A1 and MOD10A1F
111 products and derive a regional threshold for daily binary snow-covered maps in Scandinavia.
112 Wildlife camera trap networks have underutilized potential for satellite validation that could be a
113 valuable supplement to traditional validation methods based on other satellites (Crawford, 2015;
114 Huang et al., 2011), weather stations, and ground collection (Negi et al., 2007). Cameras provide
115 environmental monitoring (Brown et al., 2016; Sonnentag et al., 2012), with visual information
116 about environmental conditions along with a timestamp. While single cameras have a limited
117 field of view, they can be set up in networks of up to many hundreds of cameras across large
118 regions (Forrester et al., 2016; Garvelmann et al., 2013). Databases are increasingly available to
119 archive camera images across networks, furthering the potential for global camera networks to
120 improve environmental monitoring (Steenweg et al., 2017). For example, Wildlife Insights
121 currently hosts over 35 million images from 20,000 camera deployments worldwide
122 (<https://www.wildlifeinsights.org/home>). Cameras operate below cloud cover and tree canopy,
123 and they are particularly advantageous for monitoring snow cover because they can operate for
124 months or years in sub-freezing conditions and difficult-to-reach locations (Tobler et al., 2015).

125 Wildlife camera traps have been used successfully to evaluate satellite measures of
126 greenness (Sun et al., 2021) and to provide information on snowpack dynamics at localized

127 spatial scales (Hofmeester et al. 2021; Sirén et al., 2018). Hofmeester et al. (2021) visually
128 categorized snow cover from camera trap images to assess changes in spring and autumn molting
129 of mountain hare (*Lepus timidus*). Sirén et al. (2018) found strong correlations between depth
130 readings on snow poles and data from the Snow Data Assimilation System (SNODAS) at 80
131 cameras in Vermont. However, extracting information from camera images can be challenging.
132 Camera traps use an infrared flash in low light settings, resulting in grey-scale images that can
133 make differentiating among objects more difficult (Beery et al., 2020). Camera traps therefore
134 have great potential but require more work investigating their utility as ground-based remote
135 sensing networks for monitoring snow at broader scales.

136 Using three years of camera trap images from a network of 1,181 cameras in Norway and
137 Sweden managed by the Norwegian Institute for Nature Research (NINA), we compared snow
138 data extracted from camera images to MOD10A1 and MOD10A1F NDSI snow cover products.
139 We quantified agreement between snow cover values from cameras and MODIS NDSI,
140 examining factors we hypothesized *a priori* would affect agreement. We predicted the following:

- 141 1. Agreement would be higher between cameras and NDSI at extreme values for snow
142 cover, whereas agreement would be lower when the snow is patchy (i.e., moderate
143 NDSI values) due to differences in scales between MODIS pixels (500 m) and
144 camera fields of view (~20-80 m).
- 145 2. Factors that have been shown to affect MODIS accuracy will affect camera and
146 MODIS agreement, such that agreement will be lower when canopy cover and
147 latitude are higher (Xiao et al., 2022; Xin et al., 2012).

- 148 3. Factors that have been shown to affect image quality will affect camera and MODIS
149 agreement, such that images with low lighting taken in grey-scale (i.e., with infrared
150 flash) will have lower agreement with NDSI than images taken in full color.
- 151 4. Camera observations should agree more with MODIS observations on clear sky days
152 compared to cloudy days, and cloud persistence should decrease the agreement
153 between cameras and the cloud gap filled NDSI product.

154 We derived a binary MOD10A1 product of snow cover, using camera data to identify a NDSI
155 threshold corresponding to snow presence.

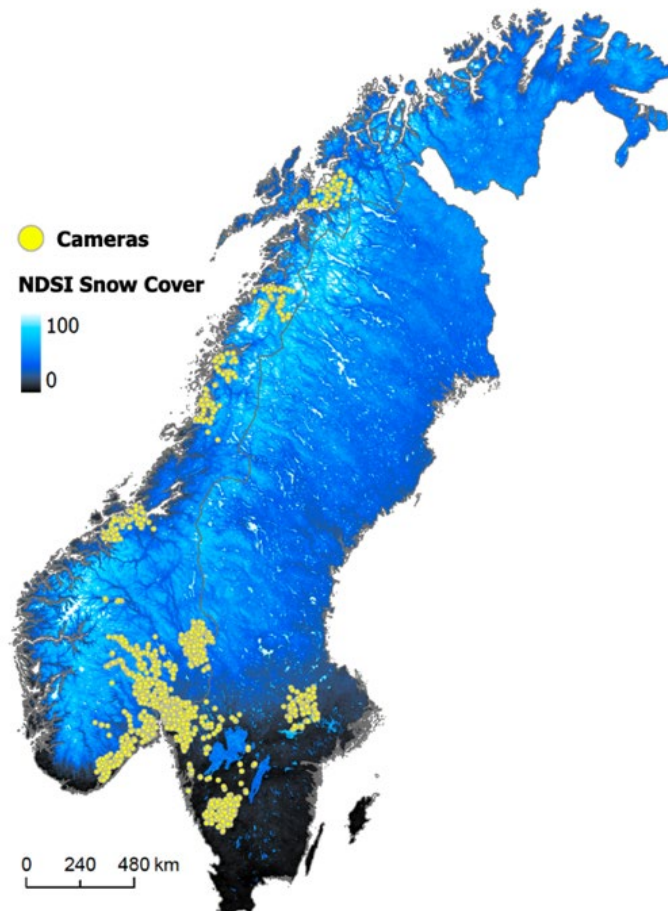
156

157 **2. Methods**

158 **2.1. Study Area**

159 We used images from camera traps in the Scandcam network. Scandcam is a long-term,
160 year-round study established in 2010 by the Norwegian Institute for Nature Research to monitor
161 recovering Eurasian lynx (*Lynx lynx*). Our dataset includes images from three winter seasons: 1)
162 January 1 – March 2018, 2) October 1, 2018 – March 2019, and 3) October 2019 – March 2020.
163 Scandcam camera trap locations are optimized for lynx detection across Norway and southern
164 Sweden (59° – 69° N, 8° – 16° E), with no more than one camera per 2 km² area across a
165 350,000 km² area (Fig. 1; Carricondo-Sanchez et al., 2017). Cameras span a 10° latitudinal
166 gradient, with deeper snow generally occurring in the north and inland than along the coast
167 (Saloranta, 2012). Snow usually arrives in Norway and Sweden in early October at high
168 elevations and northern areas and melts by early April, although sites farther north can remain
169 snow-covered into summer (Saloranta, 2012). Because the cameras were deployed to detect lynx,

170 they were placed in lynx habitat such as forests and sub-alpine areas, but they varied in whether
171 they were under closed-canopy or open-canopy areas. Southern Norway and Sweden are
172 characterized by boreal coniferous forest dominated by Norway spruce (*Picea abies*) and Scots
173 pine (*Pinus sylvestris*). In the north, forest composition transitions to alpine vegetation
174 dominated by birch species (*Betula pendula* and *Betula pubescens*) (Bouyer et al., 2015).
175
176



177

Breen, Catherine; Vuyovich, Carrie; Odden, John; Hall, Dorothy; Prugh, Laura.
Evaluating MODIS snow products using an extensive wildlife camera network. *Remote Sensing of Environment* 2023 ;Volum 295. s. - [10.1016/j.rse.2023.113648](https://doi.org/10.1016/j.rse.2023.113648)

178 Figure 1. Locations of Scandcam cameras (yellow points, $n = 1,181$) in Norway and Sweden shown over a
179 composite snow cover map created from MOD10A1 Version 6 that shows mean NDSI snow cover values across the
180 three winters of this study (January – March 2018, October 2018 – April 2019, October 2019 – April 2020).

181

182 2.2. Data

183 2.2.1. MODIS data

184 NDSI values were extracted at all camera locations ($n = 1,181$) for all days in the study
185 period from the MOD10A1 product on the Google Earth Engine public data archive ($n = 770$
186 days; Hall et al., 2016). To quantify the percentage of usable MOD10A1 NDSI values during our
187 study period, we divided the number of non-null NDSI values by the total number of values
188 (including cloud-masked pixels with “NA” values). The MOD10A1F product was downloaded
189 as GeoTiffs for the same days from the EarthData platform (<https://search.earthdata.nasa.gov/>)
190 and uploaded to Google Earth Engine (GEE). MOD10A1F NDSI and corresponding cloud
191 persistence values were extracted for all cameras for the same days after ensuring both MODIS
192 products matched projections (Appendix A1). Since MOD10A1F is not offered in the GEE
193 archive, MOD10A1F was uploaded as individual tiles. In total, we processed 3,392 tiles for the
194 MOD10A1F product. We used the GEE Collection 6 MOD10A1 product rather than Collection
195 6.1 from EarthData, because Collection 6 is commonly used in other studies, and GEE has limits
196 on the number of original assets one can store on the server. We used Collection 6.1 for
197 MOD10A1F (cloud-gap filled) NDSI and cloud persistence products to make use of the most up-
198 to-date version. Previous work has demonstrated that Collection 6.1 and Collection 6 have 99%
199 correspondence, with revisions considered minor (Riggs et al., 2019).

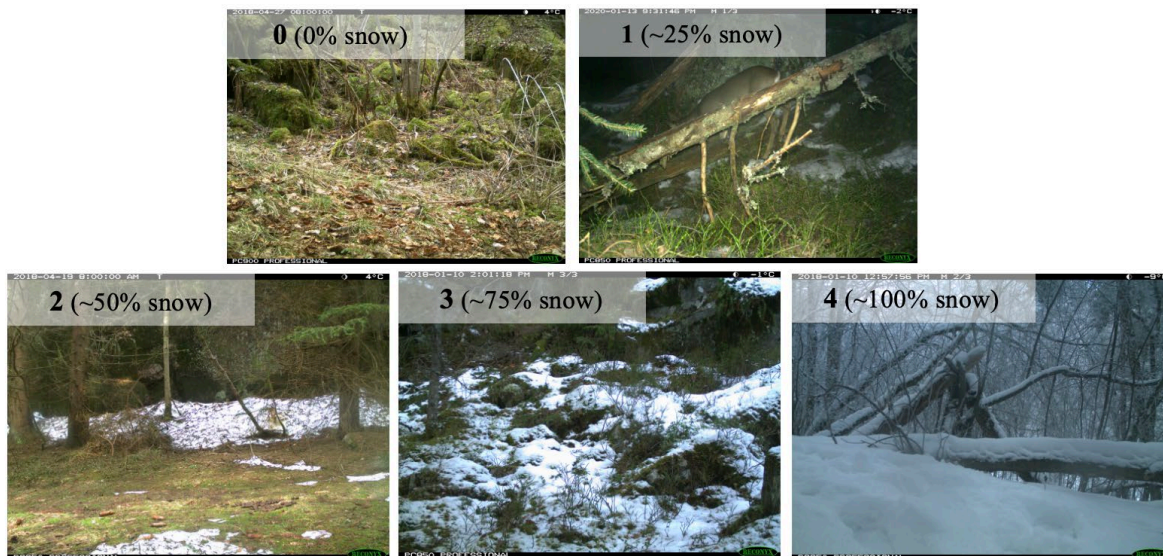
200

201 2.2.2. Camera images

202 Cameras with either infrared flash or white flash (Reconyx model HC500, HC600,
203 PC800, or PC900) were secured to trees approximately 1 m above the ground. Cameras were
204 programmed to take a daily “timelapse” image at 8 AM or 12 AM, as well as anytime the camera
205 was triggered by motion (e.g., from an animal walking by). For all cameras, for every day in our
206 study years that there was a corresponding non-null MOD10A1 value, we selected one image per
207 day from the Scandcam image inventory. The vast majority of photos were taken under low-light
208 conditions resulting in a grey-scale image. To achieve a more balanced dataset to evaluate the
209 effect of image color mode on snow labeling accuracy, we manually inspected all of the images
210 to select a color image if available. We deferred to the timelapse image when taken in white flash
211 or daylight hours, or a daytime motion-triggered image, when available. Images from the prior
212 day or the day after the image of interest were also inspected and labeled if it was hard to discern
213 snow due to lighting conditions.

214 To assess the effects of cloud cover, we labeled a subset of images that corresponded to
215 250 random days from the MOD10A1F product (100 days for each of the full winter seasons,
216 and 50 days for the partial season). Additionally, we included images that were inspected while
217 labeling MOD10A1 images ($n = 510$ images). These included both before and after images
218 corresponding to MOD10A1 values to help confirm the amount of snow. While there is
219 potentially a bias that these images would favor lower cloud persistence values, we examined a
220 histogram and found a similar distribution of cloud persistence values compared to the
221 distribution of cloud persistence values from the full MOD10A1F dataset (Appendix A2).

222 Images were labeled using Timelapse (<http://saul.cpsc.ucalgary.ca/time-lapse/>), a freely
223 available camera trap labeling software for wildlife ecologists. The software automatically
224 extracts metadata including time and date, and it provides a customizable interface that observers
225 use to label photos. All data can then be exported as a .csv file. Snow cover was manually
226 labelled using the software's user interface on an ordinal scale that ranged from 0 (no snow) to 4
227 (full snow coverage). These categories matched those used for snow cover classification at
228 Norwegian weather stations (Lussana et al., 2018): 0 corresponded to 0% snow cover, 1 to ~25%
229 snow cover, 2 to ~50%, 3 to ~75%, and 4 to ~100% (Fig. 2). Images were initially labeled by
230 two people, but testing of a double-labeled subset revealed low agreement among observers
231 (kappa coefficient $\kappa = 0.45$; McHugh, 2012). There was complete agreement at label 0, moderate
232 agreement for values 1 – 3 ($\kappa = 0.51$) and low agreement for label 4 ($\kappa = 0.10$). The low
233 agreement at label 4 was a result of the less-experienced labeler incorrectly labelling low-light
234 images with snow as “no snow.” Thus, the more-experienced observer (C. B.) labeled all images.



235

Breen, Catherine; Vuyovich, Carrie; Odden, John; Hall, Dorothy; Prugh, Laura.
Evaluating MODIS snow products using an extensive wildlife camera network. *Remote Sensing of Environment* 2023 ;Volum 295. s. - [10.1016/j.rse.2023.113648](https://doi.org/10.1016/j.rse.2023.113648)

236 Figure 2. Example remote camera images for snow classification. Snow cover was classified using an ordinal scale
237 from 0 – 4, where 0 = 0% snow cover, 1 = ~25%, 2 = ~50%, 3 = ~75%, and 4 = ~100%.

238

239 2.3. Assessing agreement between camera images and MODIS snow values

240 To evaluate the relationship between image labels and MOD10A1 (H1), we fit a general
241 linear model using the ordinal image labels as a continuous predictor variable and MOD10A1
242 NDSI as the response variable. Since NDSI values have been noted to “plateau” at higher snow
243 values depending on the normalized difference vegetation index (NDVI) at that pixel (Klein et
244 al., 1998), a polynomial term was included to account for potential non-linearity. All models
245 were fit using program R (version 4.2.1).

246 To test our prediction that agreement between MODIS and images would be highest at
247 extreme values (H1), we compared agreement between MODIS NDSI snow cover values and
248 snow cover from labeled camera images (hereafter called “image labels”) across the ordinal
249 image labels. We calculated agreement as:

$$250 \quad \text{Agreement} = 100 - |MODIS - Camera| \quad (1)$$

251 Where *MODIS* is the NDSI value and *Camera* is the labeled image value after converting
252 ordinal labels (0-4) to their corresponding percent cover values (0, 25, 50, 75, and 100).

253 Agreement could range from 0 (i.e., complete disagreement) to 100 (i.e., complete agreement).

254 Some amount of disagreement was expected from comparing ordinal image labels to continuous

255 NDSI values. Thus, we caution that agreement levels should not be compared directly to R^2

256 values from traditional validations. Other studies that assessed MODIS NDSI accuracy using

257 cameras and other ground sources converted NDSI values to binary snow and no snow values

258 using a threshold and confusion matrix (Thapa et al., 2019; Zhang et al., 2019). We made use of
 259 the full range of NDSI values by not thresholding the values for agreement assessment, in order
 260 to statistically assess covariates that affected the level of agreement. We equate NDSI to a scale
 261 of 0-100% snow cover to represent the relationship between NDSI and snow cover in the
 262 absence of factors that may affect satellite accuracy. Taking the absolute value of agreement
 263 allowed for clearer interpretation of how different covariates affected the magnitude of
 264 disagreement regardless of its direction (see 2.4). We expected agreement to be highest at the
 265 extremes (i.e., labels ~0% and ~100%) and lowest for intermediate labels (i.e., labels ~25%,
 266 50%, and 75%), so we fit a linear model with a polynomial term to allow for a parabolic shape.
 267

268 *2.4. Assessing agreement between MODIS snow products and factors influencing agreement*

269 To identify factors affecting agreement between snow cover from image labels and the
 270 MOD10A1 product (H2 and H3), we used a general linear mixed-effects model to determine
 271 how tree canopy cover, latitude (a proxy for solar zenith), and image color mode affected the
 272 agreement between image labels and MOD10A1 NDSI values (Table 1; Eqn. 2). We first tested
 273

Table 1. Covariates used to analyze agreement between MODIS and image-labeled snow values. Range of each factor is provided. MODIS cloud persistence values were only used to assess MOD10A1F (i.e., the cloud-gap filled product) agreement with camera images.

| Covariate | Range | Resolution | Hypothesized effect on agreement |
|---------------------------|------------|------------|---|
| Daily MODIS NDVI | -1.0 – 1.0 | 500 m | Increasing vegetation will prevent MODIS obs., decreasing agreement with ground obs. |
| Landsat tree canopy cover | 0 – 100% | 30 m | Increasing tree canopy cover will prevent MODIS obs., decreasing agreement with ground obs. |

| | | | |
|-------------------------|-----------------------------|----------------------|--|
| Image color mode | Color (1) or Grey-scale (0) | 20-30 m ¹ | The infrared red flash will decrease the saturation of the image (converting it to grey-scale), increasing the difficulty of differentiating snow from other aspects of the landscape. |
| Latitude | 59.0 – 69.0 | 1 degree | Increasing latitude increases angle of MODIS obs., increasing angular distortion and decreasing agreement with ground obs. |
| MODIS Cloud Persistence | 0 – 40 days | 500 m | Increasing cloud cover days increases possibility of missed accumulation or melt events, decreasing agreement with ground obs. |

¹ Resolution derived from the approximate range that wildlife cameras detect (Urbanek et al., 2019).

274
275 covariates for correlation to avoid overfitting the model. We used Pearson’s method for
276 correlation between continuous variables and Kendall’s method for correlation between
277 continuous and our categorical variable (i.e., image color mode) and found that all correlations
278 were below the commonly-used threshold of 0.7 (Dormann et al., 2013; Appendix A3). All
279 correlations were also below the threshold for moderate correlations ($|r| = 0.4$), except for tree
280 canopy cover and latitude, which was -0.404. To further examine multicollinearity among
281 predictors, we implemented the variance inflation factor (VIF) test. All factors were below 1.2,
282 lower than the conservative threshold of 3 (Zuur et al., 2010; Appendix A4). Temporal and
283 spatial autocorrelation in snow datasets can inflate parameter estimates and type 1 error
284 (Reinking et al., 2022). To evaluate spatial autocorrelation, we conducted Moran’s I test using
285 the *spdep* package in R (Bivand, 2022). We failed to detect spatial autocorrelation (Moran’s I
286 statistic = -0.007, $p = 0.55$), but we included Camera ID as a random effect to account for lack of
287 independence among images taken from the same camera. To test for temporal autocorrelation,

Breen, Catherine; Vuyovich, Carrie; Odden, John; Hall, Dorothy; Prugh, Laura.
Evaluating MODIS snow products using an extensive wildlife camera network. *Remote Sensing of Environment* 2023 ;Volum 295. s. - [10.1016/j.rse.2023.113648](https://doi.org/10.1016/j.rse.2023.113648)

288 we followed the approach of Sirén et al. (2018), and created a relative date variable for each
289 observation using the *timeDate* package in R (Wuertz et al., 2023). The package contains a
290 function to convert a date to a relative number of days from a specified origin, defaulting to
291 January 1, 1970. We tested for improved model fit using Akaike Information Criterion (AIC)
292 values with and without including the relative date in an auto-regressive correlation structure
293 (i.e., an “*ar1*” term) with camera station ID included as a grouping variable. Incorporating the
294 *ar1* correlation structure had a lower AIC score [$\Delta\text{AIC} = -1830.2$ compared to the model
295 without a correlation structure]. We therefore proceeded to use this structure for modeling
296 agreement in Eqn. (2). We included all covariates in a general linear mixed effects model with a
297 Gaussian family using the *glmmTMB* package in R (Brooks et al., 2023):

$$\begin{aligned} \text{Agreement} \sim & (1 \mid \text{Camera ID}) + \text{daily NDVI} + \text{Tree Canopy Cover} + \text{Latitude} + \\ & \text{Image Color Mode} + \text{ar1}(\text{relative date} + 0 \mid \text{Camera ID}) \end{aligned}$$

300 Agreement was calculated as described above in Eqn. (1). Image color mode was
301 classified as “Color” or “Grey-scale” by inspecting image saturation. Images taken with infrared
302 flash have low light saturation and appear as black-and-white, grey-scale images (Fig. 3). After
303 inspecting a histogram of saturation values from a subset of 60 images, there was a clear break
304 between images in grey-scale and color at saturation values of 0.02 (Appendix A5). ⁽²⁾ We then
305 evaluated this threshold using a random subset of 1,000 images and found 100% accuracy, so we
306 labeled all images with values below 0.02 as grey-scale and above 0.02 as color.



307

308 Figure 3. A grey-scale and color image from the camera on 22 November 2018 illustrates how light saturation
309 affects the ability of an observer to identify snow cover. The image on left was the daily timelapse photo taken at
310 08:00h during low light conditions, which triggered the camera to take the image in grey-scale (i.e., with infrared
311 flash). The image on the right was triggered by a wolf (*Canis lupus*) passing by at 14:03h, when there was enough
312 light for a color image. The amount of snow in the color image is much easier to see.

313

314 Previous studies found that dense forests affected MODIS NDSI by causing an
315 underestimation of the snow cover, using daily NDVI as a proxy for forest canopy (Hall and
316 Riggs, 2007; Klein et al., 1998). MODIS NDVI is a vegetation index that provides information
317 on vegetation canopy greenness, along with leaf area, and chlorophyll and canopy structure
318 (Didan, 2015). NDVI in Norway varies spatially due to differences in vegetation from boreal,
319 deciduous trees in southern Norway to alpine shrubs in northern Norway. Within a winter
320 season, NDVI is highest in October and November and lowest in February and March, likely
321 reflecting both deciduous trees losing canopy leaves in the fall, and seasonal snow covering
322 ground vegetation in January to March (Appendix A6). To test the efficacy of NDVI as a proxy
323 for tree canopy cover, we extracted the corresponding daily MODIS NDVI value at 500-m for
324 each labeled image. We also extracted tree canopy cover from the 30-m Landsat Vegetation

325 Continuous Fields tree cover layer, which estimates the percentage of horizontal ground covered
326 by woody vegetation greater than 5 meters in height from 2015 (Townshend, 2016). Continuous
327 predictor variables – tree canopy cover, latitude, and NDVI – were normalized by subtracting by
328 the mean and dividing by the standard deviation. Model fit was evaluated by examining residuals
329 for dispersion and outliers from the *DHARMA* package in R (Hartig, 2022; Appendix A9).

330 To test our prediction that agreement between MODIS and camera data would decline as
331 the number of cloudy days (i.e., cloud persistence) increased (H4), we modeled the agreement
332 between snow cover from image labels and the MOD10A1F product as a function of the cloud
333 persistence value. Because we expected the relationship between agreement and the number of
334 cloudy days to be non-linear, we ran a generalized additive mixed model with camera ID
335 included as a random effect using the *mgcv* package in R (Eqn. 3; Wood, 2017). We selected
336 eight knots for the model, following recommendations for knots to be larger than the degrees of
337 freedom (i.e., 6) plus 1 (Wood, 2017). Cloud persistence values equal to 0 (MOD10A1 values)
338 were included to allow agreement comparison to clear sky days.

$$339 \quad \text{Agreement} \sim (1 \mid \text{Camera ID}) + \text{MOD10A1F Cloud Persistence} \quad (3)$$

340 Agreement was calculated as described in 2.3 (Eqn. 1). Data was sparse for persistence
341 times > two weeks, (3% of data), so we limited analysis to 14 days.

342

343 2.5 Deriving a threshold for daily binary snow mapping in Norway

344 Image labels were converted from the 5-class ordinal scale to a binary classification by
345 reclassifying all images labeled 1 – 4 as “snow” (with a corresponding 1 label), and all image
346 labeled with a 0 as “no snow” (with a corresponding 0 label). We identified an optimal threshold

347 for the MOD10A1 product by counting the number of true positives and false positives when
348 converting to a binary product at each NDSI value. We plotted the true positive rate against the
349 false positive rate at each threshold value to create a receiver-operating-characteristic (ROC)
350 curve using the *pROC* package in R (Robin et al., 2011). The top left corner of the ROC curve is
351 known as Youden's Index, or the maximum difference between the true positive and false
352 positive rate (Youden, 1950). Because it weighs both true positive and false positive rates
353 equally, it is considered the optimum threshold for a classifier when there is equal preference for
354 both classes (Liu, 2012). In addition to generating a threshold for all cameras, we repeated this
355 analysis separately for cameras within closed canopy (> 20% canopy cover; $n = 6,229$ images)
356 and open canopy ($\leq 20\%$ cover; $n = 2,731$ images) because thresholds tend to be lower in areas
357 of closed canopy cover (Chokmani et al., 2010).

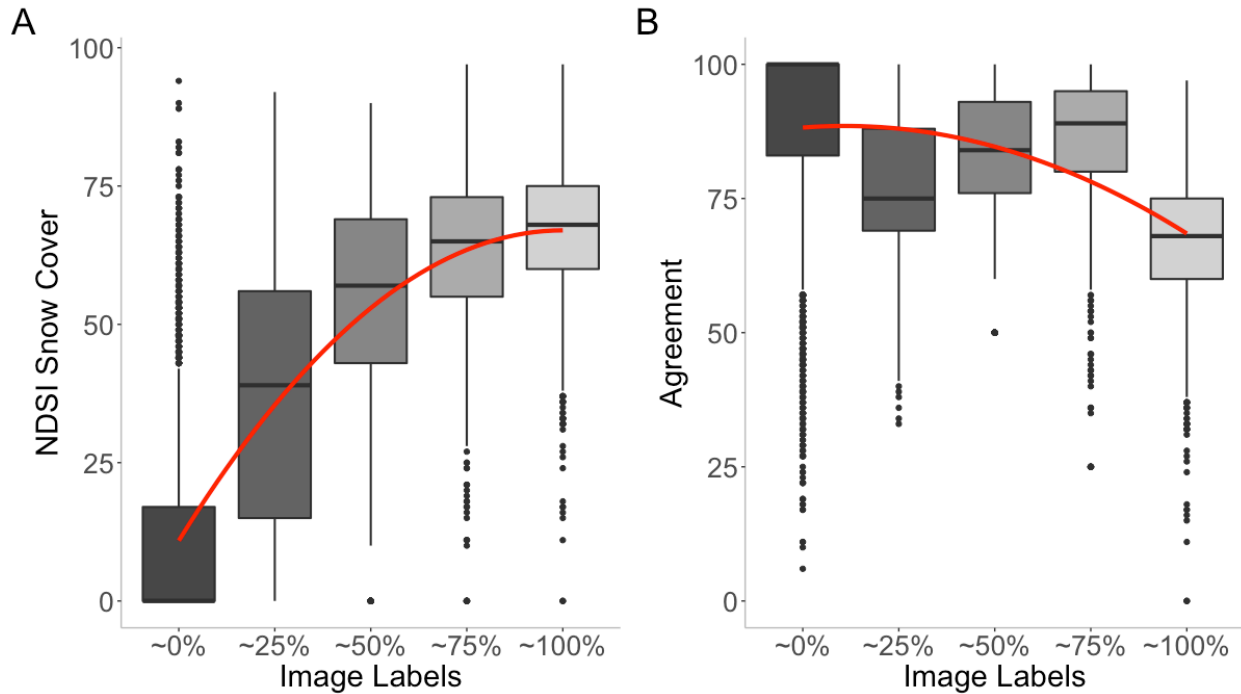
358

359 **3. Results**

360 *3.1. Labeled image and MODIS comparisons*

361 Of the 1,703,702 MOD10A1 snow cover values obtained at all 1,181 cameras during
362 winters 2018 – 2020, 1,311,249 (76%) were null (cloud-masked). Daily labeled images
363 corresponding to non-null values from MOD10A1 spanned 665 cameras ($n = 8,918$ images).
364 Cameras not included either had no corresponding non-null MODIS value or did not have
365 images on file during our study period. There was a strong correlation between snow
366 classification from the images and MOD10A1 NDSI values ($R^2 = 0.70$, $NDSI = -3.50*image^2 +$
367 $28.02*image + 10.90$, where *image* is the labeled value on the 0 - 4 scale), but the NDSI values
368 from MODIS products plateaued at about 75 (Fig. 4A). We found overall strong agreement

369 between snow cover from MODIS NDSI and camera images ($\bar{x} = 80.5\%$, 95% CI = 80.1 – 80.8;
 370 Fig. 4B). Consistent with H1, agreement was highest for images with label 0 (corresponding to
 371 ~0% snow cover; agreement $\bar{x} = 89.2\%$, 95% CI = 88.6 – 89.8). Contrary to H1, however,
 372 agreement was lowest for images with label 4 (corresponding to ~100% snow cover; agreement \bar{x}
 373 = 67.1%, 95% CI = 66.7 – 67.5, Fig. 4B).



374
 375 Figure 4. A) Distribution of MOD10A1 NDSI values within each snow cover classification from labeled camera
 376 images, and B) agreement of snow cover values between MODIS and images within each snow cover classification.
 377 Images were labeled using an ordinal classification with 5 levels (0 – 4) corresponding to snow cover percentages
 378 shown. Agreement was defined as 100 minus the absolute difference between the image label and MOD10A1 NDSI
 379 snow value. Red lines show the best fit using linear models with polynomial terms.

380

381 *3.2 Factors that influence agreement between cameras and MODIS*

382 As predicted by H3, latitude and tree canopy cover negatively affected agreement
383 between snow cover derived from cameras and MOD10A1. However, only canopy cover had a
384 statistically significant effect (Table 2). Although significant, the effect was relatively weak, and
385 mapping the agreement at each camera relative to tree canopy cover showed that agreement was
386 high in many areas with closed canopies (Fig. 5A-D). Contrary to expectations, NDVI was not
387 strongly correlated with tree canopy cover ($r = 0.09$, Appendix A3) and had a significant positive
388 effect on agreement: image labels and MODIS-derived snow cover were in better agreement in
389 areas with higher daily NDVI. Average NDVI values in October were twice as high as any other
390 month (Appendix A6), and October likewise had a relatively high proportion of 0 values with
391 high agreement (Fig. 4B). Thus, we examined the effect of removing October observations from
392 our model and found the effect of NDVI on agreement changed from strongly positive
393 (coefficient value = 6.60) to weakly negative (coefficient = -0.075; Appendix A7). Our dataset
394 was roughly split between color ($n = 4,184$ images) and grey-scale ($n = 4,733$ images), and
395 image color mode positively affected agreement as predicted by H4 (Table 2).

396

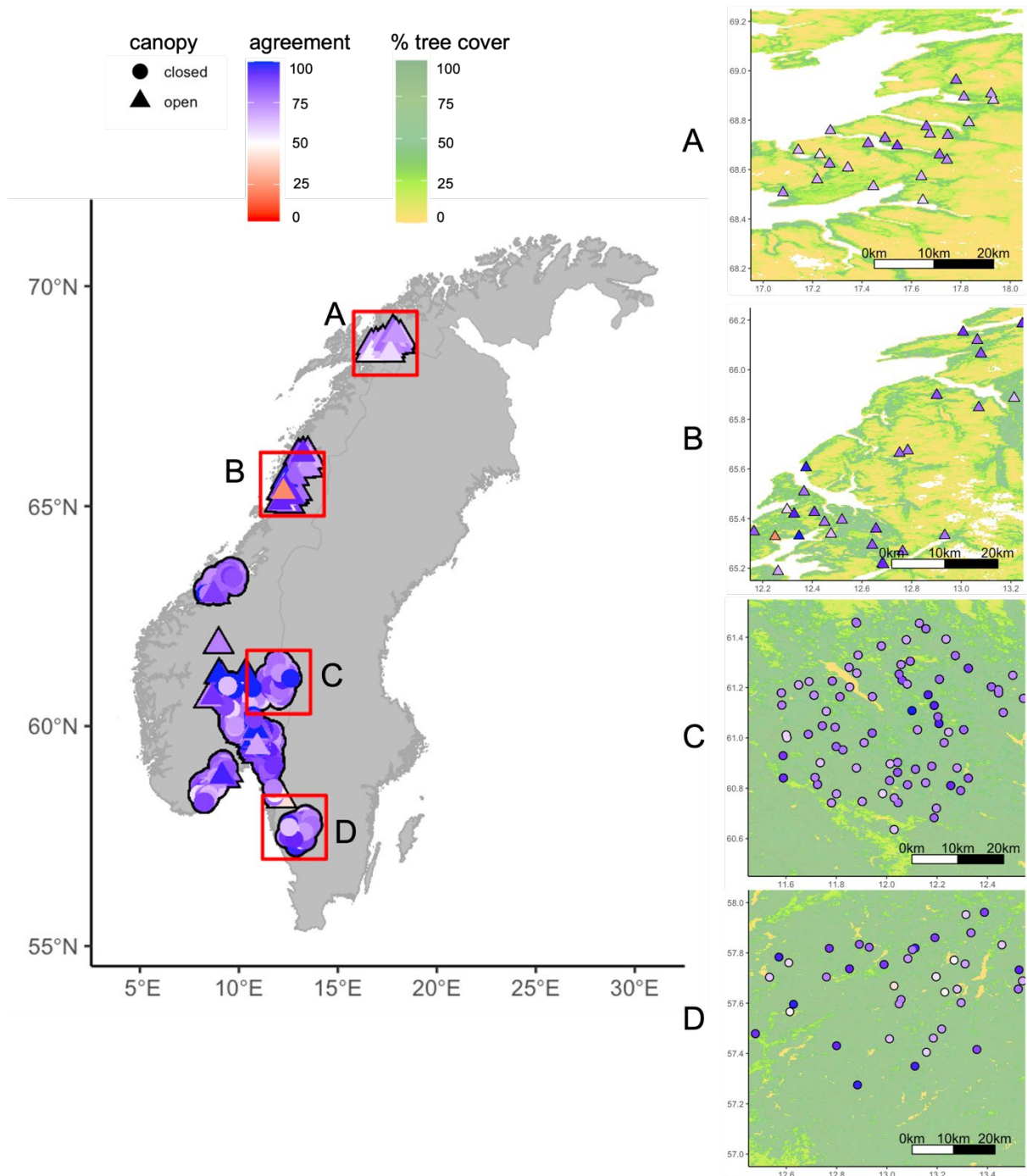
397 Table 2. Coefficient estimates, standard error (SE), t-values, and p -values from a general linear mixed model
398 assessing factors that affect MODIS and camera agreement ($n = 8,808$) for the three winter seasons: 1) January 1 -
399 March 2018, 2) October 1, 2018 – March 2019, and 3) October 2019 – March 2020. Continuous variables were
400 normalized by subtracting the mean and dividing by the standard deviation prior to analysis. Image color mode is a
401 categorical variable (1: color image; 0: grey-scale image). Camera identification was included as a random effect (n
402 = 658). Model results without observations from October 2018 and October 2019 are included in Appendix A7.
403 Results from the model without October data are similar, except that the effect size of NDVI changes from strongly
404 positive to weakly negative.

| Parameter | Estimate | SE | t-value | p-value |
|-----------------------------------|----------|------|---------|---------|
| Intercept | 78.88 | 0.40 | 196.37 | <0.005 |
| Latitude | -0.48 | 0.35 | -1.37 | 0.17 |
| NDVI | 6.60 | 0.35 | 29.12 | <0.005 |
| Tree canopy cover | -0.93 | 0.32 | -2.84 | <0.005 |
| Image color mode (color image) | 1.73 | 0.47 | 3.63 | <0.005 |

405

406

Breen, Catherine; Vuyovich, Carrie; Odden, John; Hall, Dorothy; Prugh, Laura.
Evaluating MODIS snow products using an extensive wildlife camera network. *Remote Sensing of Environment* 2023 ;Volum 295. s. - [10.1016/j.rse.2023.113648](https://doi.org/10.1016/j.rse.2023.113648)



407

408

Figure 5. Average agreement between snow cover from labeled images and MOD10A1 snow cover at Scandcam

409

cameras between winter months for 2018 – 2020. The four boxes correspond to four example clusters in counties

410

from north to south: A) north Nordland and Troms og Finnmark; B) south Nordland; C) Innlandet; and D) south

Breen, Catherine; Vuyovich, Carrie; Odden, John; Hall, Dorothy; Prugh, Laura.
 Evaluating MODIS snow products using an extensive wildlife camera network. *Remote Sensing of Environment* 2023 ;Volum 295. s. - [10.1016/j.rse.2023.113648](https://doi.org/10.1016/j.rse.2023.113648)

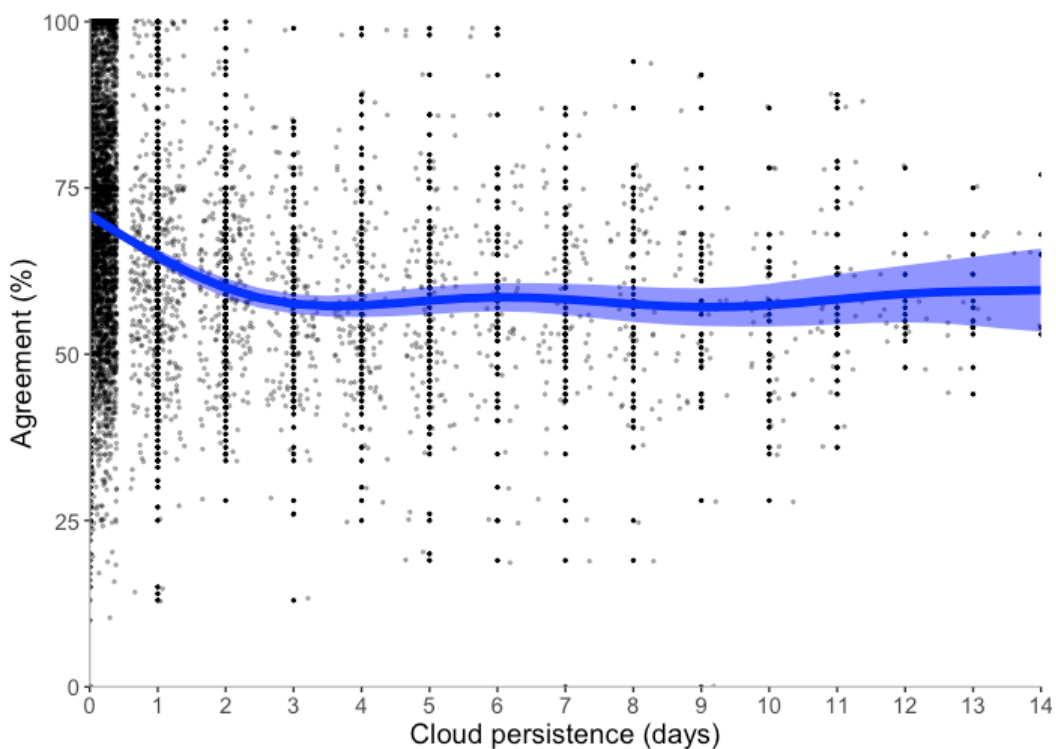
411 Viken. The base map is tree canopy cover from 30-m Landsat. Triangles represent cameras within closed canopy
412 areas ($\geq 20\%$) and circles represent cameras within open canopy areas ($< 20\%$).

413

414 3.3 Image labels and MOD10A1F product comparison

415 Cloud persistence was a significant predictor for agreement between image labels and
416 snow values from the MOD10A1F product. Agreement was highest (78.5%) on clear sky days
417 (i.e. cloud persistence = 0) and decreased by almost one third (to 56.4%) within the first 3 days
418 before leveling off just after (Fig. 6).

419



420

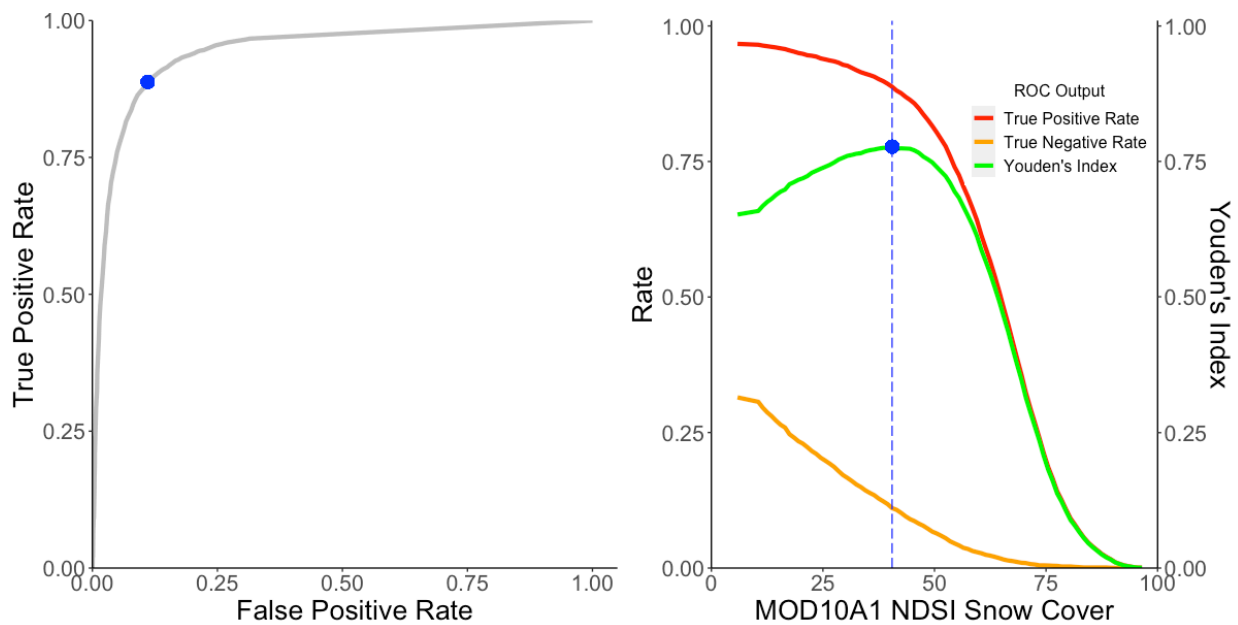
421 Figure 6. Agreement between image labels and MOD10A1F NDSI snow values as a function of number of cloudy
422 days (i.e., cloud persistence) using a generalized additive model. Agreement was defined as 100 minus the absolute
423 difference between the image label and MOD10A1F NDSI snow value.

Breen, Catherine; Vuyovich, Carrie; Odden, John; Hall, Dorothy; Prugh, Laura.
Evaluating MODIS snow products using an extensive wildlife camera network. *Remote Sensing of Environment* 2023 ;Volum 295. s. - [10.1016/j.rse.2023.113648](https://doi.org/10.1016/j.rse.2023.113648)

424

425 3.4. Optimal threshold derivation for binary snow cover mapping

426 At the Youden's Index point of the ROC curve, the true positive rate was 88% and the false
427 positive rate was 11%. This point corresponded to a MOD10A1 NDSI snow cover value of 40.5
428 (Figure 7). At the commonly used threshold value of 40 (Hall et al., 2019a), the true positive rate
429 was 89% and the false positive rate was 11%, showing that for a slightly higher true positive
430 rate, there is not much difference in the false positive rate. The current MOD10A2 product
431 employs a threshold of 10, which has a 97% true positive rate and 31% false negative rate. When
432



433

434 Figure 7: A) A Receiver-Operator Characteristic (ROC) curve when images are reclassified for snow or no-snow by
435 cutting the data with a label ≥ 1 as 'snow.' The ROC curve shows the performance of the classifier at each
436 threshold, in this case the value of the NDSI snow cover. The closer the curve is to the top left corner, the better the
437 performance of the model. The blue point closest to the top left corner is (0.11, 0.88) is referred to as Youden's
438 Index. B) The true negative rate (orange) and the true positive rate (red) graphed separately for every MOD10A1

439 NDSI snow cover value alongside the Youden's Index, the difference in between (green). The MOD10A1 value at
440 the maximum value of the Youden index is 40.50. The maximum value of the Youden index is the minimum
441 between the true positive rate and true negative rate when both classes are given equal weight. The blue points on
442 both graphs represent the same cut point in the data.

443 we conducted separate analyses for closed canopy ($\geq 20\%$) and open canopy ($< 20\%$) sites, the
444 threshold was the same for closed canopy locations (40.5) and slightly higher for open canopy
445 locations (41.5). Appendix A8 shows the change in true positive and false positive rates with
446 different threshold values, along with the results for open and closed canopy analyses.

447

448 **Discussion**

449 In this study, we identified strong agreement between snow information obtained from
450 wildlife cameras and MODIS at a regional scale, demonstrating the ability of cameras to
451 supplement MODIS snow observations. Previous studies have found strong agreement using
452 fewer than 100 cameras in tandem with satellites at localized spatial scales (Raleigh et al., 2013;
453 Sugiura et al., 2013), and our findings show this relationship holds across a large region and
454 multiple winter seasons. As predicted, we found strongest agreement at low snow cover values,
455 but agreement was worse than expected at high snow cover values because NDSI values
456 plateaued around 75 instead of 100. Cameras, thus, demonstrated that an NDSI value of 75
457 represents 100% snow cover for this region. We also demonstrated the ability to customize
458 MOD10A1 to create binary snow maps using a camera-derived threshold of 40.5, which was
459 nearly identical to the commonly used 40 threshold from previous MODIS products (Klein et al.,
460 1998). These findings highlight that despite large differences in scales, wildlife camera networks

461 have potential to improve satellite monitoring for snow and create new products at fine temporal
462 scales.

463 Our finding of strong agreement between camera image snow values and MODIS snow
464 values may be attributed in part to our method of classifying snow cover into five classes. While
465 not a continuous measure, a 5-class ordinal labeling scheme for images extracts more
466 information about the amount of snow cover than previous work using binary labels (Berman et
467 al., 2018; Sugiura et al., 2013). There are caveats to this classification scheme, as agreement was
468 lower at labels 1 (i.e., ~25% snow cover), 2 (i.e., ~50%), and 4 (i.e., ~100%), which may
469 highlight MODIS uncertainties. For example, MODIS is less accurate when snow is thin or
470 patchy, such as labels 1 and 2 (Berman et al., 2018; Dong and Menzel, 2016). Similarly, low
471 agreement at label 4 highlights the tendency of MODIS to underestimate snow cover in boreal
472 regions (Klein et al., 1998). In this region, maximum NDSI equating to 100% snow cover
473 appears to be 75, when MODIS plateaus. Cameras can thus be used to adjust NDSI for fractional
474 snow-covered maps. However, discrepancies in agreement at different classification schemes
475 highlights drawbacks to using cameras in tandem with satellite products: patchy snow in cameras
476 may be missed or interpreted as complete snow cover. Furthermore, labeling for snow cover
477 values can be subjective and have uncertainty, as highlighted by low correspondence among
478 labels by two observers found during pilot testing. We recommend a single, experienced labeler
479 when labeling wildlife photos, and testing for agreement among labelers early on. Despite lower
480 agreement within certain classes and among observers, strong agreement overall suggests that
481 cameras can be an effective method of snow classification when used in tandem with satellites.

482 We predicted that latitude (i.e., solar zenith angles), ground vegetation, and the image
483 color mode (i.e., grey or color scale) would limit MODIS and camera image agreement (Xiao et
484 al., 2022; Xin et al., 2012). Although mapping the agreement at each of our cameras showed a
485 general decline in agreement as latitude increased, the effect was not significant, and there was
486 still strong agreement even at high latitudes. Overall, our findings indicated that latitude and
487 canopy cover had relatively minor effects on the accuracy of MODIS snow cover, highlighting
488 its robustness for monitoring snow trends across Scandinavia. Images in grey-scale had lower
489 overall agreement with satellites, and they took much longer to label due to the need to study the
490 image more carefully to separate snow from vegetation and rocks. Humans and artificial
491 intelligence have more difficulty extracting information about environmental conditions and
492 wildlife from grey-scale images (Beery et al., 2019; Favorskaya and Buryachenko, 2019).
493 Nighttime images are inevitable when using motion-triggered wildlife cameras for environmental
494 monitoring, but we recommend maximizing the number of color images either through
495 prioritizing color photos as we did here, or by scheduling timelapse photos to occur during
496 daylight hours. Because low-light images were also the main reason why images from one
497 labeler had to be relabeled, prioritizing color photos may increase both agreement between
498 camera and satellite as well as agreement among labelers.

499 Using cameras to assess agreement demonstrated drawbacks of using NDVI alongside
500 MODIS NDSI. Contrary to our hypothesis, NDVI positively affected the agreement. While daily
501 NDVI is often included to account for the effects of vegetation on MODIS snow detection (Hall
502 et al., 2002; Klein et al., 1998; Xin et al., 2012), NDVI has multiple interpretations, including
503 green-up, biomass, and plant stress (Huang et al., 2021). The positive effect of NDVI on snow

504 cover agreement suggests that daily NDVI during winter may not have represented vegetation
505 that was obscuring the sensor, but rather the absence of snow. We included snow values ranging
506 from 0 – 100, but values equal to 0 for both camera images and MODIS will have exact
507 agreement whereas our estimates for the other snow labels were approximations. When we
508 excluded images from the month October, the month that also has the highest average NDVI at
509 the camera locations, we found the expected negative relationship between NDVI and agreement
510 for months between November and March. October data was important to include in our study
511 because the “snow-on” date typically occurs during October in Norway, and this date is critical
512 for deriving snow cover phenology metrics used by wildlife ecologists studying migration timing
513 and other seasonal phenomena. However, the strong effect of October on the NDVI estimate
514 reinforces that NDVI was reflecting the absence of snow rather than canopy cover. We also
515 examined maximum NDVI over each snow-covered season as a covariate instead of daily NDVI,
516 and we found similar results (Appendix A7). In contrast, the tree canopy cover covariate had a
517 negative effect on agreement as expected, even with October data included. The Landsat tree
518 canopy cover product is a more direct measure of obstructing vegetation than NDVI (Potapov et
519 al., 2021; Sexton et al., 2013), and our findings indicate that direct canopy products may be
520 preferable to NDVI for snow mapping applications.

521 Agreement was also affected by cloudy days, supporting previous literature on limitations
522 of cloud-gap filled products in cloudy regions (Gao et al., 2011; Hall et al., 2019b). However,
523 agreement did not decrease linearly with time, but instead decreased rapidly and then leveled off
524 after 3 days. This result is likely due to clouds changing the snow conditions, such as
525 snowstorms increasing snow cover or increased humidity accelerating snowmelt (Zhang et al.,

526 1996). Backfilling pixels with the most recent cloud-free value thus has limitations even for short
527 cloud persistence durations. In cases when clouds persist for much of the winter, our results
528 show that gap-filled products may be highly inaccurate, and wildlife camera data in these regions
529 is especially valuable. While cloud-masked MOD10A1 values had substantially higher
530 agreement with camera images than gap-filled MOD10A1F values, use of the MOD10A1
531 product comes at the cost of substantial data loss, as only 23% of pixels were usable due to cloud
532 masking. Similarly, a study examining how snow properties affect movements of GPS-collared
533 Dall sheep (*Ovis dalli dalli*) in Lake Clark National Park, Alaska, was only able to use 2.2% of
534 their dataset when using cloud-masked MODIS products (Mahoney et al., 2018). Ultimately,
535 spatial products of snow cover may be able to automate the inclusion of snow values from
536 camera networks when satellite values are not accurate or available, utilizing AI and machine
537 learning to produce spatially and temporally fill gaps.

538 Gap-filling accuracy with camera-labeled values will depend on classification accuracy,
539 and image classification error may be further reduced by using a binary classification, although
540 some information is lost. However, binary maps can be especially useful for identifying snow-on
541 and snow-off dates, with important applications for monitoring changing snow phenology and
542 impacts on seasonal migrations and breeding seasons. The threshold NDSI value of 40.5 we
543 identified using wildlife cameras in Scandinavia was remarkably similar to the value of 40
544 derived for MODIS from Landsat fractional snow-covered area maps in Canada (Klein et al.,
545 1998). Thresholds in forested areas tend to be lower than open canopy thresholds because some
546 snow visibility is blocked by the trees (Chokmani et al., 2010). Our findings were consistent with
547 these trends, but the effect of canopy cover was minor (40.5 vs 41.5 for closed vs open canopy

Breen, Catherine; Vuyovich, Carrie; Odden, John; Hall, Dorothy; Prugh, Laura.
Evaluating MODIS snow products using an extensive wildlife camera network. *Remote Sensing
of Environment* 2023 ;Volum 295. s. - [10.1016/j.rse.2023.113648](https://doi.org/10.1016/j.rse.2023.113648)

548 sites, respectively). By employing Youden’s index to select the optimal threshold, we assumed
549 equal weight to both snow and no snow classes. However, depending on the mapping needs,
550 other threshold values could be used. For example, higher thresholds for snow might be desirable
551 when making maps of the first “snow on” date in the fall to prioritize snow detection. Other
552 studies have found adjustments to the threshold can increase regional accuracy (Chokmani et al.,
553 2010; Da Ronco et al., 2020; Luo et al., 2022). While our study found that MODIS detected 88%
554 of snow-covered pixels, Luo et al. (2022) found that MODIS identified just 14-18% of snow-
555 covered pixels in forests when using conventional MODIS thresholds. MODIS snow detection
556 tends to be less accurate in steep areas with complex topography (Rittger et al., 2021), and the
557 Luo et al. (2022) study occurred in alpine terrain with sites > 2700 m a.s.l. and slopes between 19
558 and 34 degrees. Our study occurred at much lower elevations (0 – 800 m a.s.l.), with moderate
559 slopes between 0.5 to 20 degrees. These differences reinforce our findings that agreement
560 between camera and satellite may depend on environmental factors, and when using the two for
561 validation or in-tandem, it is important to account for external context. Generally, a threshold of
562 40 is robust for this region, similar to other studies creating binary maps from forested
563 ecosystems. A threshold of 10 from MOD10A2 would be low for this region, thus researchers
564 should be aware that deriving their own binary thresholds is an important step for MODIS
565 Collection 6 products. Future studies could employ this approach to create custom thresholds
566 from cameras in their regions of interest.

567 Because our cameras were optimized for lynx detection, we did not control for field of
568 view. Previous work suggests that wider field of views are more advantageous for snow cover
569 monitoring (Parajka et al., 2012). Our results suggest that even narrow fields of view offer

570 insight into snow conditions, but wider fields should provide a better observation of snow
571 conditions at a scale more similar to satellite remote sensing. Additionally, we did not control for
572 possible observation delays, which could be up to 24 hours depending on when the satellite
573 passes over the area of interest and when the camera image is taken (Sugiura et al., 2013). One
574 camera trap image per day appeared sufficient to connect to MODIS, but we recommend
575 multiple images per camera each day to increase labeling options. Examining the outliers from
576 our model evaluations aligns with these recommendations, because outlier images consisted
577 primarily of those with narrow fields of view and active weather (Appendix A9). Continuous
578 indices of vegetation greenness have been derived from camera images using RGB values as
579 proxies for vegetation (Sun et al., 2021), but to our knowledge, no automated method of
580 extracting continuous snow cover indices from camera images has been developed. AI
581 algorithms for automated snow detection from camera images are a promising area of
582 development to increase the utility of wildlife camera networks for environmental monitoring.

583 Our study focused on comparing snow cover from cameras to MODIS snow products, and
584 we found surprisingly strong agreement considering differences in spatial resolution. The Visible
585 Infrared Imaging Radiometer Suite (VIIRS) instrument has a snow product similar to MODIS at
586 375-m spatial resolution (Riggs et al., 2017). Future work could explore incorporating multiple
587 cameras in one satellite pixel to improve snow monitoring of patchy snow conditions, such as
588 during snow accumulation and snow melt. Alternatively, camera images could be matched to
589 finer-resolution snow products derived from satellites such as Landsat, Sentinel, and Planet
590 CubeSat (Cannistra et al., 2021; Chokmani et al., 2010, 2010; Riggs et al., 2017). Snow maps
591 must be derived by manually creating the NDSI maps from Landsat, Sentinel, and Planet

Breen, Catherine; Vuyovich, Carrie; Odden, John; Hall, Dorothy; Prugh, Laura.
Evaluating MODIS snow products using an extensive wildlife camera network. *Remote Sensing
of Environment* 2023 ;Volum 295. s. - [10.1016/j.rse.2023.113648](https://doi.org/10.1016/j.rse.2023.113648)

592 sensors, but these products have spatial resolutions at 30 m, 10 m, and 0.7-3 m, respectively,
593 closer to the camera field of view (Cannistra et al., 2021).

594

595 **Conclusion**

596 As the remote sensing community continues to develop new global products, the wildlife
597 ecology community continues to expand camera trap networks for continuous biodiversity
598 monitoring (Pettorelli et al., 2014; Steenweg et al., 2017). Connecting camera traps to satellite
599 data represents an important step towards an interconnected network of ground-based remote
600 sensing data that can improve researchers' and the public's ability to determine environmental
601 changes and subsequent impacts on sensitive species. In Norway, snow cover extent has
602 decreased by more than 20,000 km² (6% of the country area) since 1961 due to changes in
603 temperature and precipitation (Rizzi et al., 2018; Skaugen et al., 2012). When these trends are
604 incorporated into climate impact models, predictions suggest accelerated rates of local
605 extinctions across 273 species of Norwegian vegetation (Niittynen et al., 2018). With the
606 increasing number of cameras operating as environmental monitoring devices, we can improve
607 our understanding of both environmental and wildlife responses in a changing climate.

608

609

610

611

612

613

614

615 **Data Availability**

616 A selection of photos is publicly available at <https://viltkamera.nina.no>. Analysis code can be
617 found at [https://github.com/catherine-m-breen/MODIS-Snow-Cover-to-Binary-Snow-Covered-](https://github.com/catherine-m-breen/MODIS-Snow-Cover-to-Binary-Snow-Covered-Area)
618 [Area](#). GEE assets are available at the following links:

619 https://code.earthengine.google.com/?asset=users/catherinembreen/MODIS_Norway

620

621 **Description of author's responsibilities**

622 LRP and CB conceived of the idea. CB labeled images, ran statistical analyses, and led the
623 writing. JO managed camera data and provided data access. DH and CV provided remote sensing
624 expertise. All authors edited the manuscript.

625

626 **Acknowledgements:** We thank Sunniva Bahlk, Nina Myhr, Solveig Haug, for help in obtaining
627 Scandcam images. Calum Cunningham and provided useful comments on preliminary drafts and
628 analytical considerations, and members of the Prugh Lab provided valuable feedback on
629 manuscript drafts.

630

631 **Funding:** This research was supported by the Erasmus Mobility + Exchange as well as NASA
632 Graduate Fellowship Program Grant # 80NSSC19K1673. The Scandcam project was supported
633 by the Norwegian Environment Agency, the Research Council of Norway (grants 251112 and
634 281092).

635

Breen, Catherine; Vuyovich, Carrie; Odden, John; Hall, Dorothy; Prugh, Laura.
Evaluating MODIS snow products using an extensive wildlife camera network. *Remote Sensing of Environment* 2023 ;Volum 295. s. - [10.1016/j.rse.2023.113648](https://doi.org/10.1016/j.rse.2023.113648)

636 **References**

- 637 Beery, S., Wu, G., Rathod, V., Votel, R., Huang, J., 2019. Long Term Temporal Context for Per-
638 Camera Object Detection. ArXiv191203538 Cs Eess Q-Bio.
- 639 Berman, E.E., Bolton, D.K., Coops, N.C., Mityok, Z.K., Stenhouse, G.B., Moore, R.D. (Dan),
640 2018. Daily estimates of Landsat fractional snow cover driven by MODIS and dynamic
641 time-warping. *Remote Sens. Environ.* 216, 635–646.
642 <https://doi.org/10.1016/j.rse.2018.07.029>
- 643 Bivand, R., 2022. R Packages for Analyzing Spatial Data: A Comparative Case Study with Areal
644 Data. *Geogr. Anal.* 54, 488–518. <https://doi.org/10.1111/gean.12319>
- 645 Boelman, N.T., Liston, G.E., Gurarie, E., Meddens, A.J.H., Mahoney, P.J., Kirchner, P.B.,
646 Bohrer, G., Brinkman, T.J., Cosgrove, C.L., Eitel, J.U.H., Hebblewhite, M., Kimball,
647 J.S., LaPoint, S., Nolin, A.W., Pedersen, S.H., Prugh, L.R., Reinking, A.K., Vierling,
648 L.A., 2019. Integrating snow science and wildlife ecology in Arctic-boreal North
649 America. *Env. Res. Lett.* 14, 010401. <https://doi.org/10.1088/1748-9326/aaec1>
- 650 Bokhorst, S., 2016. Changing Arctic snow cover: A review of recent developments and
651 assessment of future needs for observations, modelling, and impacts 22.
- 652 Bouyer, Y., San Martin, G., Poncin, P., Beudels-Jamar, R.C., Odden, J., Linnell, J.D.C., 2015.
653 Eurasian lynx habitat selection in human-modified landscape in Norway: Effects of
654 different human habitat modifications and behavioral states. *Biol. Conserv.* 191, 291–
655 299. <https://doi.org/10.1016/j.biocon.2015.07.007>
- 656 Brooks, M., E., Kristensen, K., Benthem, K., J., van, Magnusson, A., Berg, C., W., Nielsen, A.,

Breen, Catherine; Vuyovich, Carrie; Odden, John; Hall, Dorothy; Prugh, Laura.
Evaluating MODIS snow products using an extensive wildlife camera network. *Remote Sensing of Environment* 2023 ;Volum 295. s. - [10.1016/j.rse.2023.113648](https://doi.org/10.1016/j.rse.2023.113648)

657 Skaug, H., J., Mächler, M., Bolker, B., M., 2017. glmmTMB Balances Speed and
658 Flexibility Among Packages for Zero-inflated Generalized Linear Mixed Modeling. The
659 R Journal 9, 378. <https://doi.org/10.32614/RJ-2017-066>

660 Brown, R.D., Mote, P.W., 2009. The Response of Northern Hemisphere Snow Cover to a
661 Changing Climate. J. Clim. 22, 2124–2145. <https://doi.org/10.1175/2008JCLI2665.1>

662 Brown, T.B., Hultine, K.R., Steltzer, H., Denny, E.G., Denslow, M.W., Granados, J., Henderson,
663 S., Moore, D., Nagai, S., SanClements, M., Sánchez-Azofeifa, A., Sonnentag, O., Tazik,
664 D., Richardson, A.D., 2016. Using phenocams to monitor our changing Earth: toward a
665 global phenocam network. Front. Ecol. Environ. 14, 84–93.
666 <https://doi.org/10.1002/fee.1222>

667 Cannistra, A.F., Shean, D.E., Cristea, N.C., 2021. High-resolution CubeSat imagery and machine
668 learning for detailed snow-covered area. Remote Sens. Environ. 258, 112399.
669 <https://doi.org/10.1016/j.rse.2021.112399>

670 Carricondo-Sanchez, D., Odden, M., Linnell, J.D.C., Odden, J., 2017. The range of the mangle:
671 Spatiotemporal patterns of sarcoptic mange in red foxes (*Vulpes vulpes*) as revealed by
672 camera trapping. PLoS ONE 12, e0176200.
673 <https://doi.org/10.1371/journal.pone.0176200>

674 Chokmani, K., Dever, K., Bernier, M., Gauthier, Y., Paquet, L.-M., 2010. Adaptation of the
675 SNOWMAP algorithm for snow mapping over eastern Canada using Landsat-TM
676 imagery. Hydrol. Sci. J. 55, 649–660. <https://doi.org/10.1080/02626661003747374>

Breen, Catherine; Vuyovich, Carrie; Odden, John; Hall, Dorothy; Prugh, Laura.
Evaluating MODIS snow products using an extensive wildlife camera network. *Remote Sensing of Environment* 2023 ;Volum 295. s. - [10.1016/j.rse.2023.113648](https://doi.org/10.1016/j.rse.2023.113648)

677 Coll, J., Li, X., 2018. Comprehensive accuracy assessment of MODIS daily snow cover products
678 and gap filling methods. *ISPRS J. Photogramm. Remote Sens.* 144, 435–452.
679 <https://doi.org/10.1016/j.isprsjprs.2018.08.004>

680 Crawford, C.J., 2015. MODIS Terra Collection 6 fractional snow cover validation in
681 mountainous terrain during spring snowmelt using Landsat TM and ETM+. *Hydrol.*
682 *Process.* 29, 128–138. <https://doi.org/10.1002/hyp.10134>

683 Curk, T., Pokrovsky, I., Lecomte, N., Aarvak, T., Brinker, D.F., Burnham, K., Dietz, A., Dixon,
684 A., Franke, A., Gauthier, G., Jacobsen, K.-O., Kidd, J., Lewis, S.B., Øien, I.J., Sokolov,
685 A., Sokolov, V., Solheim, R., Weidensaul, S., Wiebe, K., Wikelski, M., Therrien, J.-F.,
686 Safi, K., 2020. Arctic avian predators synchronise their spring migration with the
687 northern progression of snowmelt. *Sci. Rep.* 10, 7220. [https://doi.org/10.1038/s41598-](https://doi.org/10.1038/s41598-020-63312-0)
688 [020-63312-0](https://doi.org/10.1038/s41598-020-63312-0)

689 Da Ronco, P., Avanzi, F., De Michele, C., Notarnicola, C., Schaepli, B., 2020. Comparing
690 MODIS snow products Collection 5 with Collection 6 over Italian Central Apennines.
691 *Int. J. Remote Sens.* 41, 4174–4205. <https://doi.org/10.1080/01431161.2020.1714778>

692 Didan, K., 2015. MOD13A1 MODIS/Terra Vegetation Indices 16-Day L3 Global 500m SIN
693 Grid V006. NASA LP DAAC. <https://doi.org/10.5067/MODIS/MOD13A1.006>

694 Dong, C., Menzel, L., 2016. Producing cloud-free MODIS snow cover products with conditional
695 probability interpolation and meteorological data. *Remote Sens. Environ.* 186, 439–451.
696 <https://doi.org/10.1016/j.rse.2016.09.019>

697 Dormann, C.F., Elith, J., Bacher, S., Buchmann, C., Carl, G., Carré, G., Marquéz, J.R.G.,
698 Gruber, B., Lafourcade, B., Leitão, P.J., Münkemüller, T., McClean, C., Osborne, P.E.,

Breen, Catherine; Vuyovich, Carrie; Odden, John; Hall, Dorothy; Prugh, Laura.
Evaluating MODIS snow products using an extensive wildlife camera network. *Remote Sensing of Environment* 2023 ;Volum 295. s. - [10.1016/j.rse.2023.113648](https://doi.org/10.1016/j.rse.2023.113648)

699 Reineking, B., Schröder, B., Skidmore, A.K., Zurell, D., Lautenbach, S., 2013.
700 Collinearity: a review of methods to deal with it and a simulation study evaluating their
701 performance. *Ecography* 36, 27–46. <https://doi.org/10.1111/j.1600-0587.2012.07348.x>
702 Favorskaya, M., Buryachenko, V., 2019. Selecting Informative Samples for Animal Recognition
703 in the Wildlife, in: Czarnowski, I., Howlett, R.J., Jain, L.C. (Eds.), *Intelligent Decision*
704 *Technologies 2019, Smart Innovation, Systems and Technologies*. Springer Singapore,
705 Singapore, pp. 65–75. https://doi.org/10.1007/978-981-13-8303-8_6
706 Forrester, T., O'Brien, T., Fegraus, E., Jansen, P., Palmer, J., Kays, R., Ahumada, J., Stern, B.,
707 McShea, W., 2016. An Open Standard for Camera Trap Data. *Biodivers. Data J.* 4,
708 e10197. <https://doi.org/10.3897/BDJ.4.e10197>
709 Franklin, S.E., 2020. Interpretation and use of geomorphometry in remote sensing: a guide and
710 review of integrated applications. *Int. J. Remote Sens.* 41, 7700–7733.
711 <https://doi.org/10.1080/01431161.2020.1792577>
712 Gao, Y., Lu, N., Yao, T., 2011. Evaluation of a cloud-gap-filled MODIS daily snow cover
713 product over the Pacific Northwest USA. *J. Hydrol.* 404, 157–165.
714 <https://doi.org/10.1016/j.jhydrol.2011.04.026>
715 Garvelmann, J., Pohl, S., Weiler, M., 2013. From observation to the quantification of snow
716 processes with a time-lapse camera network. *Hydrol. Earth Syst. Sci.* 17, 1415–1429.
717 <https://doi.org/10.5194/hess-17-1415-2013>
718 Hall, D.K., Kelly, R.E.J., Riggs, G.A., Chang, A.T.C., Foster, J.L., 2002. Assessment of the
719 relative accuracy of hemispheric-scale snow-cover maps. *Ann. Glaciol.* 34, 24–30.
720 <https://doi.org/10.3189/172756402781817770>

Breen, Catherine; Vuyovich, Carrie; Odden, John; Hall, Dorothy; Prugh, Laura.
Evaluating MODIS snow products using an extensive wildlife camera network. *Remote Sensing of Environment* 2023 ;Volum 295. s. - [10.1016/j.rse.2023.113648](https://doi.org/10.1016/j.rse.2023.113648)

721 Hall, D.K., Riggs, G.A., 2007. Accuracy assessment of the MODIS snow products. *Hydrol.*
722 *Process.* 21, 1534–1547. <https://doi.org/10.1002/hyp.6715>

723 Hall, D.K., Riggs, G.A., DiGirolamo, N.E., Román, M.O., 2019a. MODIS Cloud-Gap Filled
724 Snow-Cover Products: Advantages and Uncertainties (preprint). *Snow and Ice/Remote*
725 *Sensing and GIS.* <https://doi.org/10.5194/hess-2019-123>

726 Hall, D.K., Riggs, G.A., DiGirolamo, N.E., Román, M.O., 2019b. Evaluation of MODIS and
727 VIIRS cloud-gap-filled snow-cover products for production of an Earth science data
728 record. *Hydrol. Earth Syst. Sci.* 23, 5227–5241. [https://doi.org/10.5194/hess-23-5227-](https://doi.org/10.5194/hess-23-5227-2019)
729 2019

730 Hall, D.K., Riggs, G.A., Foster, J.L., Kumar, S.V., 2010. Development and evaluation of a
731 cloud-gap-filled MODIS daily snow-cover product. *Remote Sens. Environ.* 114, 496–
732 503. <https://doi.org/10.1016/j.rse.2009.10.007>

733 Hall, D. K., Riggs G., A., Solomonson, V., 2016. MODIS/Terra Snow Cover Daily L3 Global
734 500m SIN Grid, Version 6. Boulder, Colorado USA. NASA National Snow and Ice Data
735 Center Distributed Active Archive Center.
736 <https://doi.org/10.5067/MODIS/MOD10A1.006>

737 Hao, X., Huang, G., Zheng, Z., Sun, X., Ji, W., Zhao, H., Wang, J., Li, H., Wang, X., 2022.
738 Development and validation of a new MODIS snow-cover-extent product over China.
739 *Hydrol. Earth Syst. Sci.* 26, 1937–1952. <https://doi.org/10.5194/hess-26-1937-2022>

740 Hartig, F., 2022. DHARMA: Residual Diagnostics for Hierarchical (Multi-Level / Mixed)
741 Regression Models. R package version 0.4.6. [https://CRAN.R-](https://CRAN.R-project.org/package=DHARMA)
742 [project.org/package=DHARMA](https://CRAN.R-project.org/package=DHARMA)

Breen, Catherine; Vuyovich, Carrie; Odden, John; Hall, Dorothy; Prugh, Laura.
Evaluating MODIS snow products using an extensive wildlife camera network. *Remote Sensing of Environment* 2023 ;Volum 295. s. - [10.1016/j.rse.2023.113648](https://doi.org/10.1016/j.rse.2023.113648)

743 Hofmeester, T.R., Young, S., Juthberg, S., Singh, N.J., Widemo, F., Andrén, H., Linnell, J.D.C.,
744 Cromsigt, J.P.G.M., 2019. Using by-catch data from wildlife surveys to quantify climatic
745 parameters and the timing of phenology for plants and animals using camera traps.
746 *Remote Sens Ecol Conserv* rse2.136. <https://doi.org/10.1002/rse2.136>

747 Huang, S., Tang, L., Hupy, J.P., Wang, Y., Shao, G., 2021. A commentary review on the use of
748 normalized difference vegetation index (NDVI) in the era of popular remote sensing. *J.*
749 *For. Res.* 32, 1–6. <https://doi.org/10.1007/s11676-020-01155-1>

750 Huang, X., Liang, T., Zhang, X., Guo, Z., 2011. Validation of MODIS snow cover products
751 using Landsat and ground measurements during the 2001–2005 snow seasons over
752 northern Xinjiang, China. *Int. J. Remote Sens.* 32, 133–152.
753 <https://doi.org/10.1080/01431160903439924>

754 Klein, A.G., Hall, D.K., Riggs, G.A., 1998. Improving snow cover mapping in forests through
755 the use of a canopy reflectance model. *Hydrol. Process.* 12, 1723–1744.
756 [https://doi.org/10.1002/\(SICI\)1099-1085\(199808/09\)12:10/11<1723::AID-](https://doi.org/10.1002/(SICI)1099-1085(199808/09)12:10/11<1723::AID-HYP691>3.0.CO;2-2)
757 [HYP691>3.0.CO;2-2](https://doi.org/10.1002/(SICI)1099-1085(199808/09)12:10/11<1723::AID-HYP691>3.0.CO;2-2)

758 Laforge, M.P., Bonar, M., Vander Wal, E., 2021. Tracking snowmelt to jump the green wave:
759 phenological drivers of migration in a northern ungulate. *Ecology* 102.
760 <https://doi.org/10.1002/ecy.3268>

761 Liang, T., Huang, X., Wu, C., Liu, X., Li, W., Guo, Z., Ren, J., 2008. An application of MODIS
762 data to snow cover monitoring in a pastoral area: A case study in Northern Xinjiang,
763 China. *Remote Sens. Environ.* 112, 1514–1526. <https://doi.org/10.1016/j.rse.2007.06.001>

Breen, Catherine; Vuyovich, Carrie; Odden, John; Hall, Dorothy; Prugh, Laura.
Evaluating MODIS snow products using an extensive wildlife camera network. *Remote Sensing of Environment* 2023 ;Volum 295. s. - [10.1016/j.rse.2023.113648](https://doi.org/10.1016/j.rse.2023.113648)

764 Liu, X., 2012. Classification accuracy and cut point selection. *Stat. Med.* 31, 2676–2686.
765 <https://doi.org/10.1002/sim.4509>

766 Luo, J., Dong, C., Lin, K., Chen, X., Zhao, L., Menzel, L., 2022. Mapping snow cover in forests
767 using optical remote sensing, machine learning and time-lapse photography. *Remote*
768 *Sens. Environ.* 275, 113017. <https://doi.org/10.1016/j.rse.2022.113017>

769 Lussana, C., Saloranta, T., Skaugen, T., Magnusson, J., Tveito, O.E., Andersen, J., 2018.
770 seNorge2 daily precipitation, an observational gridded dataset over Norway from 1957 to
771 the present day. *Earth Syst. Sci. Data* 10, 235–249. [https://doi.org/10.5194/essd-10-235-](https://doi.org/10.5194/essd-10-235-2018)
772 2018

773 Madsen, J., Tamstorf, M., Klaassen, M., Eide, N., Glahder, C., Rigét, F., Nyegaard, H., Cottaar,
774 F., 2007. Effects of snow cover on the timing and success of reproduction in high-Arctic
775 pink-footed geese *Anser brachyrhynchus*. *Polar Biol.* 30, 1363–1372.
776 <https://doi.org/10.1007/s00300-007-0296-9>

777 Mahoney, P.J., Liston, G.E., LaPoint, S., Gurarie, E., Mangipane, B., Wells, A.G., Brinkman,
778 T.J., Eitel, J.U.H., Hebblewhite, M., Nolin, A.W., Boelman, N., Prugh, L.R., 2018.
779 Navigating snowscapes: scale-dependent responses of mountain sheep to snowpack
780 properties. *Ecol. Appl.* 28, 1715–1729. <https://doi.org/10.1002/eap.1773>

781 Mankin, J.S., Viviroli, D., Singh, D., Hoekstra, A.Y., Diffenbaugh, N.S., 2015. The potential for
782 snow to supply human water demand in the present and future. *Environ. Res. Lett.* 10,
783 114016. <https://doi.org/10.1088/1748-9326/10/11/114016>

784 McHugh, M.L., 2012. Interrater reliability: the kappa statistic. *Biochem Med* 276–282.
785 <https://doi.org/10.11613/BM.2012.031>

Breen, Catherine; Vuyovich, Carrie; Odden, John; Hall, Dorothy; Prugh, Laura.
Evaluating MODIS snow products using an extensive wildlife camera network. *Remote Sensing of Environment* 2023 ;Volum 295. s. - [10.1016/j.rse.2023.113648](https://doi.org/10.1016/j.rse.2023.113648)

786 Negi, H.S., Thakur, N.K., Mishra, V.D., 2007. Estimation and validation of snow surface
787 temperature using modis data for snow-avalanche studies in NW-Himalaya. *J. Indian*
788 *Soc. Remote Sens.* 35, 287–299. <https://doi.org/10.1007/BF02990785>

789 Nolin, A.W., 2010. Recent advances in remote sensing of seasonal snow. *J. Glaciol.* 56, 1141–
790 1150. <https://doi.org/10.3189/002214311796406077>

791 Niittynen, P., Heikkinen, R.K., Luoto, M., 2018. Snow cover is a neglected driver of Arctic
792 biodiversity loss. *Nature Clim Change* 8, 997–1001. [https://doi.org/10.1038/s41558-018-](https://doi.org/10.1038/s41558-018-0311-x)
793 0311-x

794 Parajka, J., Haas, P., Kirnbauer, R., Jansa, J., Blöschl, G., 2012. Potential of time-lapse
795 photography of snow for hydrological purposes at the small catchment scale:
796 POTENTIAL OF TIME-LAPSE PHOTOGRAPHY OF SNOW FOR HYDROLOGICAL
797 PURPOSES. *Hydrol. Process.* 26, 3327–3337. <https://doi.org/10.1002/hyp.8389>

798 Pettorelli, N., Laurance, W.F., O'Brien, T.G., Wegmann, M., Nagendra, H., Turner, W., 2014.
799 Satellite remote sensing for applied ecologists: opportunities and challenges. *Journal of*
800 *Applied Ecology* 51, 839–848. <https://doi.org/10.1111/1365-2664.12261>

801 Potapov, P., Li, X., Hernandez-Serna, A., Tyukavina, A., Hansen, M.C., Kommareddy, A.,
802 Pickens, A., Turubanova, S., Tang, H., Silva, C.E., Armston, J., Dubayah, R., Blair, J.B.,
803 Hofton, M., 2021. Mapping global forest canopy height through integration of GEDI and
804 Landsat data. *Remote Sens. Environ.* 253, 112165.
805 <https://doi.org/10.1016/j.rse.2020.112165>

806 Raleigh, M.S., Rittger, K., Moore, C.E., Henn, B., Lutz, J.A., Lundquist, J.D., 2013. Ground-
807 based testing of MODIS fractional snow cover in subalpine meadows and forests of the

Breen, Catherine; Vuyovich, Carrie; Odden, John; Hall, Dorothy; Prugh, Laura.
Evaluating MODIS snow products using an extensive wildlife camera network. *Remote Sensing of Environment* 2023 ;Volum 295. s. - [10.1016/j.rse.2023.113648](https://doi.org/10.1016/j.rse.2023.113648)

808 Sierra Nevada. *Remote Sens. Environ.* 128, 44–57.
809 <https://doi.org/10.1016/j.rse.2012.09.016>

810 Reinking, A.K., Højlund Pedersen, S., Elder, K., Boelman, N.T., Glass, T.W., Oates, B.A.,
811 Bergen, S., Roberts, S., Prugh, L.R., Brinkman, T.J., Coughenour, M.B., Feltner, J.A.,
812 Barker, K.J., Bentzen, T.W., Pedersen, Å.Ø., Schmidt, N.M., Liston, G.E., 2022.
813 Collaborative wildlife–snow science: Integrating wildlife and snow expertise to improve
814 research and management. *Ecosphere* 13. <https://doi.org/10.1002/ecs2.4094>

815 Riggs, G.A., Hall, D.K., Román, M.O., 2017. Overview of NASA’s MODIS and Visible Infrared
816 Imaging Radiometer Suite (VIIRS) snow-cover Earth System Data Records. *Earth Syst.*
817 *Sci. Data* 9, 765–777. <https://doi.org/10.5194/essd-9-765-2017>

818 Riggs, G.A., Hall, D.K., Román, M.O., 2019. MODIS Snow Products Collection 6.1 User Guide,
819 Version 1.0. NASA Goddard Space Flight Center. [https://modis-snow-ice-](https://modis-snow-ice-gsfc.nasa.gov/?c=userguides)
820 [gsfc.nasa.gov/?c=userguides](https://modis-snow-ice-gsfc.nasa.gov/?c=userguides)

821 Rittger, K., Bormann, K.J., Bair, E.H., Dozier, J., Painter, T.H., 2021. Evaluation of VIIRS and
822 MODIS Snow Cover Fraction in High-Mountain Asia Using Landsat 8 OLI. *Front.*
823 *Remote Sens.* 2, 647154. <https://doi.org/10.3389/frsen.2021.647154>

824 Rizzi, J., Nilsen, I.B., Stagge, J.H., Gislås, K., Tallaksen, L.M., 2018. Five decades of warming:
825 impacts on snow cover in Norway. *Hydrol. Res.* 49, 670–688.
826 <https://doi.org/10.2166/nh.2017.051>

827 Robin, X., Turck, N., Hainard, A., Tiberti, N., Lisacek, F., Sanchez, J.-C., Müller, M., 2011.
828 pROC: an open-source package for R and S+ to analyze and compare ROC curves. *BMC*
829 *Bioinformatics* 12, 77. <https://doi.org/10.1186/1471-2105-12-77>

Breen, Catherine; Vuyovich, Carrie; Odden, John; Hall, Dorothy; Prugh, Laura.
Evaluating MODIS snow products using an extensive wildlife camera network. *Remote Sensing of Environment* 2023 ;Volum 295. s. - [10.1016/j.rse.2023.113648](https://doi.org/10.1016/j.rse.2023.113648)

830 Saloranta, T.M., 2012. Simulating snow maps for Norway: description and statistical evaluation
831 of the seNorge snow model. *The Cryosphere* 6, 1323–1337. [https://doi.org/10.5194/tc-6-](https://doi.org/10.5194/tc-6-1323-2012)
832 1323-2012

833 Sexton, J.O., Song, X.-P., Feng, M., Noojipady, P., Anand, A., Huang, C., Kim, D.-H., Collins,
834 K.M., Channan, S., DiMiceli, C., Townshend, J.R., 2013. Global, 30-m resolution
835 continuous fields of tree cover: Landsat-based rescaling of MODIS vegetation continuous
836 fields with lidar-based estimates of error. *Int. J. Digit. Earth* 6, 427–448.
837 <https://doi.org/10.1080/17538947.2013.786146>

838 Sirén, A.P.K., Somos-Valenzuela, M., Callahan, C., Kilborn, J.R., Duclos, T., Tragert, C.,
839 Morelli, T.L., 2018. Looking beyond wildlife: using remote cameras to evaluate accuracy
840 of gridded snow data. *Remote Sens Ecol Conserv* 4, 375–386.
841 <https://doi.org/10.1002/rse2.85>

842 Skaugen, T., Strandén, H.B., Saloranta, T., 2012. Trends in snow water equivalent in Norway
843 (1931–2009). *Hydrology Research* 43, 489–499. <https://doi.org/10.2166/nh.2012.109>

844 Solomon, S., Qin, D., Manning, M., Marquis, M., Averyt, K., Tignor, M., LeRoy Miller, H,
845 Chen, Z., 2007. *Climate change 2007: the physical science basis: contribution of Working*
846 *Group I to the Fourth Assessment Report of the Intergovernmental Panel on Climate*
847 *Change*. Cambridge University Press, Cambridge; New York.

848 Sonnentag, O., Hufkens, K., Teshera-Sterne, C., Young, A.M., Friedl, M., Braswell, B.H.,
849 Milliman, T., O’Keefe, J., Richardson, A.D., 2012. Digital repeat photography for
850 phenological research in forest ecosystems. *Agric. For. Meteorol.* 152, 159–177.
851 <https://doi.org/10.1016/j.agrformet.2011.09.009>

Breen, Catherine; Vuyovich, Carrie; Odden, John; Hall, Dorothy; Prugh, Laura.
Evaluating MODIS snow products using an extensive wildlife camera network. *Remote Sensing of Environment* 2023 ;Volum 295. s. - [10.1016/j.rse.2023.113648](https://doi.org/10.1016/j.rse.2023.113648)

852 Steenweg, R., Hebblewhite, M., Kays, R., Ahumada, J., Fisher, J.T., Burton, C., Townsend, S.E.,
853 Carbone, C., Rowcliffe, J.M., Whittington, J., Brodie, J., Royle, J.A., Switalski, A.,
854 Clevenger, A.P., Heim, N., Rich, L.N., 2017. Scaling-up camera traps: monitoring the
855 planet's biodiversity with networks of remote sensors. *Front. Ecol. Environ.* 15, 26–34.
856 <https://doi.org/10.1002/fee.1448>

857 Sugiura, K., Nagai, S., Nakai, T., Suzuki, R., 2013. Application of time-lapse digital imagery for
858 ground-truth verification of satellite indices in the boreal forests of Alaska. *Polar Sci.* 7,
859 149–161. <https://doi.org/10.1016/j.polar.2013.02.003>

860 Sun, C., Beirne, C., Burgar, J.M., Howey, T., Fisher, J.T., Burton, A.C., 2021. Simultaneous
861 monitoring of vegetation dynamics and wildlife activity with camera traps to assess
862 habitat change. *Remote Sens. Ecol. Conserv.* 7, 666–684.
863 <https://doi.org/10.1002/rse2.222>

864 Thapa, S., Chhetri, P.K., Klein, A.G., 2019. Cross-Comparison between MODIS and VIIRS
865 Snow Cover Products for the 2016 Hydrological Year. *Climate* 7, 57.
866 <https://doi.org/10.3390/cli7040057>

867 Tobler, M.W., Zúñiga Hartley, A., Carrillo-Percegué, S.E., Powell, G.V.N., 2015.
868 Spatiotemporal hierarchical modelling of species richness and occupancy using camera
869 trap data. *J. Appl. Ecol.* 52, 413–421. <https://doi.org/10.1111/1365-2664.12399>

870 Townshend, J., 2016. Global Forest Cover Change (GFCC) Forest Cover Change Multi-Year
871 Global 30 m V001. NASA LP DAAC.
872 <https://doi.org/10.5067/MEASURES/GFCC/GFCC30FCC.001>

Breen, Catherine; Vuyovich, Carrie; Odden, John; Hall, Dorothy; Prugh, Laura.
Evaluating MODIS snow products using an extensive wildlife camera network. *Remote Sensing of Environment* 2023 ;Volum 295. s. - [10.1016/j.rse.2023.113648](https://doi.org/10.1016/j.rse.2023.113648)

873 Urbanek, R.E., Ferreira, H.J., Olfenbuttel, C., Dukes, C.G., Albers, G., 2019. See what you've
874 been missing: An assessment of Reconyx® PC900 Hyperfire cameras. *Wildl. Soc. Bull.*
875 43, 630–638. <https://doi.org/10.1002/wsb.1015>

876 Wood, S.N., 2017. *Generalized Additive Models: An Introduction with R* (2nd edition).
877 Chapman and Hall/CRC. <https://doi.org/10.1201/9781315370279>

878 Wuertz, D., Setz, T., Chalabi, Y., Boshnakov, G., 2023. timeDate: Rmetrics - Chronological and
879 Calendar Objects. R package version 4022.108. [https://CRAN.R-](https://CRAN.R-project.org/package=timeDate)
880 [project.org/package=timeDate](https://CRAN.R-project.org/package=timeDate)

881 Xiao, X., He, T., Liang, Shunlin, Liu, X., Ma, Y., Liang, Shuang, Chen, X., 2022. Estimating
882 fractional snow cover in vegetated environments using MODIS surface reflectance data.
883 *Int. J. Appl. Earth Obs. Geoinformation* 114, 103030.
884 <https://doi.org/10.1016/j.jag.2022.103030>

885 Xin, Q., Woodcock, C.E., Liu, J., Tan, B., Melloh, R.A., Davis, R.E., 2012. View angle effects
886 on MODIS snow mapping in forests. *Remote Sens. Environ.* 118, 50–59.
887 <https://doi.org/10.1016/j.rse.2011.10.029>

888 Youden, W.J., 1950. Index for rating diagnostic tests. *Cancer* 3, 32–35.
889 [https://doi.org/10.1002/1097-0142\(1950\)3:1<32::AID-CNCR2820030106>3.0.CO;2-3](https://doi.org/10.1002/1097-0142(1950)3:1<32::AID-CNCR2820030106>3.0.CO;2-3)

890 Zhang, H., Zhang, F., Zhang, G., Che, T., Yan, W., Ye, M., Ma, N., 2019. Ground-based
891 evaluation of MODIS snow cover product V6 across China: Implications for the selection
892 of NDSI threshold. *Sci. Total Environ.* 651, 2712–2726.
893 <https://doi.org/10.1016/j.scitotenv.2018.10.128>

Breen, Catherine; Vuyovich, Carrie; Odden, John; Hall, Dorothy; Prugh, Laura.
Evaluating MODIS snow products using an extensive wildlife camera network. *Remote Sensing of Environment* 2023 ;Volum 295. s. - [10.1016/j.rse.2023.113648](https://doi.org/10.1016/j.rse.2023.113648)

894 Zhang, T., Stamnes, K., Bowling, S.A., 1996. Impact of Clouds on Surface Radiative Fluxes and
895 Snowmelt in the Arctic and Subarctic. *J. Climate*. 9, 2110–2123.

896 [https://doi.org/10.1175/1520-0442\(1996\)009<2110:IOCOSR>2.0.CO;2](https://doi.org/10.1175/1520-0442(1996)009<2110:IOCOSR>2.0.CO;2)

897 Zuur, A.F., Ieno, E.N., Elphick, C.S., 2010. A protocol for data exploration to avoid common
898 statistical problems: *Data exploration*. *Methods Ecol. Evol.* 1, 3–14.

899 <https://doi.org/10.1111/j.2041-210X.2009.00001.x>

900

901

902 **List of Figure Captions**

903 Figure 1. Locations of Scandcam cameras (yellow points, $n = 1,181$) in Norway and Sweden
904 shown over a composite snow cover map created from MOD10A1 Version 6 that shows mean
905 NDSI snow cover values across the three winters of this study (January – March 2018, October
906 2018 – April 2019, October 2019 – April 2020).

907

908 Figure 2. Example remote camera images for snow classification. Snow cover was classified
909 using an ordinal scale from 0 – 4, where 0 = 0% snow cover, 1 = ~25%, 2 = ~50%, 3 = ~75%,
910 and 4 = ~100%.

911

912 Figure 3. A grey-scale and color image from the camera on 22 November 2018 illustrates how
913 light saturation affects the ability of an observer to identify snow cover. The image on left was
914 the daily timelapse photo taken at 08:00h during low light conditions, which triggered the
915 camera to take the image in grey-scale (i.e., with infrared flash). The image on the right was

916 triggered by a wolf (*Canis lupus*) passing by at 14:03h, when there was enough light for a color
917 image. The amount of snow in the color image is much easier to see.

918

919 Figure 4. A) Distribution of MOD10A1 NDSI values within each snow cover classification from
920 labeled camera images, and B) agreement of snow cover values between MODIS and images
921 within each snow cover classification. Images were labeled using an ordinal classification with 5
922 levels (0 – 4) corresponding to snow cover percentages shown. Agreement was defined as 100
923 minus the absolute difference between the image label and MOD10A1 NDSI snow value. Red
924 lines show the best fit using linear models with polynomial terms.

925

926 Figure 5. Average agreement between snow cover from labeled images and MOD10A1 snow
927 cover at Scandcam cameras between winter months for 2018 – 2020. The four boxes correspond
928 to four example clusters in counties from north to south: A) north Nordland and Troms og
929 Finnmark; B) south Nordland; C) Innlandet; and D) south Viken. The base map is tree canopy
930 cover from 30-m Landsat. Triangles represent cameras within closed canopy areas ($\geq 20\%$) and
931 circles represent cameras within open canopy areas ($< 20\%$).

932

933 Figure 6. Agreement between image labels and MOD10A1F NDSI snow values as a function of
934 number of cloudy days (i.e., cloud persistence) using a generalized additive model. Agreement
935 was defined as 100 minus the absolute difference between the image label and MOD10A1F
936 NDSI snow value.

937

938 Figure 7: A) A Receiver-Operator Characteristic (ROC) curve when images are reclassified for
939 snow or no-snow by cutting the data with a label ≥ 1 as 'snow.' The ROC curve shows the
940 performance of the classifier at each threshold, in this case the value of the NDSI snow cover.
941 The closer the curve is to the top left corner, the better the performance of the model. The blue
942 point closest to the top left corner is (0.11, 0.88) is referred to as Youden's Index. B) The true
943 negative rate (orange) and the true positive rate (red) graphed separately for every MOD10A1
944 NDSI snow cover value alongside the Youden's Index, the difference in between (green). The
945 MOD10A1 value at the maximum value of the Youden index is 40.50. The maximum value of
946 the Youden index is the minimum between the true positive rate and true negative rate when both
947 classes are given equal weight. The blue points on both graphs represent the same cut point in the
948 data.

949

950 **List of Table Captions**

951 Table 1. Covariates used to analyze agreement between MODIS and image-labeled snow values. Range of each
952 factor is provided. MODIS cloud persistence values were only used to assess MOD10A1F (i.e., the cloud-gap filled
953 product) agreement with camera images.

954

955 Table 2. Coefficient estimates, standard error (SE), t-values, and *p*-values from a general linear mixed model
956 assessing factors that affect MODIS and camera agreement ($n = 8,808$) for the three winter seasons: 1) January 1 -
957 March 2018, 2) October 1, 2018 – March 2019, and 3) October 2019 – March 2020. Continuous variables were
958 normalized by subtracting the mean and dividing by the standard deviation prior to analysis. Image color mode is a
959 categorical variable (1: color image; 0: grey-scale image). Camera identification was included as a random effect (n
960 = 658). Model results without observations from October 2018 and October 2019 are included in Appendix A7.

Breen, Catherine; Vuyovich, Carrie; Odden, John; Hall, Dorothy; Prugh, Laura.
Evaluating MODIS snow products using an extensive wildlife camera network. *Remote Sensing of Environment* 2023 ;Volum 295. s. - [10.1016/j.rse.2023.113648](https://doi.org/10.1016/j.rse.2023.113648)

961 Results from the model without October data are similar, except that the effect size of NDVI changes from strongly
962 positive to weakly negative.

963

964

965